Analysis of Nucleosome Dynamics by Fluorescence Correlation Spectroscopy

by

Kaushik Gurunathan

A Dissertation Presented in Partial Fulfillment
of the Requirements for the Degree
Doctor of Philosophy

Approved April 2011 by the
Graduate Supervisory Committee:

Marcia Levitus, Chair
Hao Yan
Stuart Lindsay
Neal Woodbury

ARIZONA STATE UNIVERSITY

May 2011

ABSTRACT

Nucleosomes are the basic repetitive unit of eukaryotic chromatin and are responsible for packing DNA inside the nucleus of the cell. They consist of a complex of eight histone proteins (two copies of four proteins H2A, H2B, H3 and H4) around which 147 base pairs of DNA are wrapped in ~1.67 superhelical turns. Although the nucleosomes are stable protein-DNA complexes, they undergo spontaneous conformational changes that occur in an asynchronous fashion. This conformational dynamics, defined by the "site-exposure" model, involves the DNA unwrapping from the protein core and exposing itself transiently before wrapping back. Physiologically, this allows regulatory proteins to bind to their target DNA sites during cellular processes like replication, DNA repair and transcription. Traditional biochemical assays have established the equilibrium constants for the accessibility to various sites along the length of the nucleosomal DNA, from its end to the middle of the dyad axis. Using fluorescence correlation spectroscopy (FCS), we have established the position dependent rewrapping rates for nucleosomes. We have also used Monte Carlo simulation methods to analyze the applicability of FRET fluctuation spectroscopy towards conformational dynamics, specifically motivated by nucleosome dynamics. Another important conformational change that is involved in cellular processes is the disassembly of nucleosome into its constituent particles. The exact pathway adopted by nucleosomes is still not clear. We used dual color fluorescence correlation spectroscopy to study the intermediates during nucleosome disassembly induced by changing ionic strength. Studying the nature

of nucleosome conformational change and the kinetics is very important in understanding gene expression. The results from this thesis give a quantitative description to the basic unit of the chromatin.

ACKNOWLEDGMENTS

I would like to thank my parents and sister for providing me with everything I needed to be here.

I would like to thank Pavithra Venkatagopalan for having supported me throughout our undergrad and grad life.

I would like to thank Professor Pennathur Gautam who said I should pursue Biophysics and here I am.

I would like to thank Professor G V Shivashankar for introducing me to experimental biophysics. And his students Aprotim and Feroz for teaching me tricks of the trade.

I would like to thank Professor Marcia Levitus for giving me this opportunity, I could not have asked for a better doctoral advisor. Thank you for guiding me at every step, both scientifically and professionally. I would also like to thank past and present members of the group: Brian Connolly, Matt Sanborn, Mahinda Ranasinghe, Tedman Torres, Billie Harvey, Suman Ranjit, Manas Chakraborty, Jennifer Binder, Elana Stennet and of course Shreya Bhattacharyya (the honorary member of Levitus lab) for giving me company through graduate school.

I would also like to thank Professor Stuart Lindsay, Professor Hao Yan and Professor Neal Woodbury for serving on my committee.

TABLE OF CONTENTS

CHAPTER Page

LIST OF FIGURES

Figure Page

Figure Page

Chapter 1

FLUORESCENCE CORRELATION SPECTROSCOPY: APPLICATIONS TO STUDY NUCLEOSOME CONFORMATIONAL DYNAMICS

Nucleosomes

Nucleosomes are the basic unit of the eukaryotic chromatin. In a eukaryotic cell, the DNA, a negatively charged polymer, is compactly packed inside the nucleus. In the case of humans, a three-billion base pair genome (roughly a meter in length if fully extended) is packaged efficiently inside a micron sized cell. Nucleosomes, whose identity was established in the 1970s[1-3], facilitate the compaction of the DNA into the cells. Fig. 1-1 shows the hierarchy of organization of DNA from the double helix to the mitotic chromosome.

High resolution X-ray structure of the nucleosome has been solved[4,5]. Each nucleosome consists of approximately 150 base pairs of DNA wrapped around a protein octamer core. This modular octamer consists of two copies of four positively charged histone proteins namely H2A, H2B, H3 and H4. Two copies of the H3 and H4 form a $(H3\text{-}H4)_2$ tetramer and two pairs of H2A-H2B heterodimer flank the tetramer on either side. All four histones are similar in structure consisting of a structured, three-helix domain called the histone fold and two non-structural tails. The tail regions are rich in positively charged amino acid residues (lysine and arginine) and are predominantly responsible for forming salt bridges with the phosphate oxygens on the DNA. These salt bridges, along with

hydrogen bonds, are formed every 10 bp when the DNA minor groove faces inward and this lack of sequence specificity leads to incorporation of any sequence within a nucleosome. However, it has been suggested that certain sequences bind with greater affinity and form more stable nucleosomes and this leads to a nucleosome positioning code and could impact regulation of cellular processes[6]. The 150 base pair DNA is wrapped around the octamer in 1.67 left-handed superhelical turns. The free energy required to bend the DNA is offset by multiple direct and water mediated interactions[4]. Nucleosomes are also sensitive to ionic strengths[7,8] and to post-translational modifications which can disrupt the electrostatic interactions[9,10]. Fig. 1-2 shows the crystal structure of the nucleosome showing the histone proteins forming the core and the DNA wrapped in left-handed superhelical turns.

Nucleosomes are linked to each other by linker DNA which varies in length depending on species and tissue type[11]. The linker DNA is stabilized by linker histones (H1 or H5). The arrangement of nucleosomes on DNA is describes as a “bead on string” model[12] and the array of nucleosomes are further compacted into higher order structures until the formation of chromosomes. The details of the higher order structures are still a debated topic and continue to be researched.

Nucleosome Dynamics

Nucleosomes are highly stable with respect to the protein-DNA interaction. However they are not completely static and are known to undergo

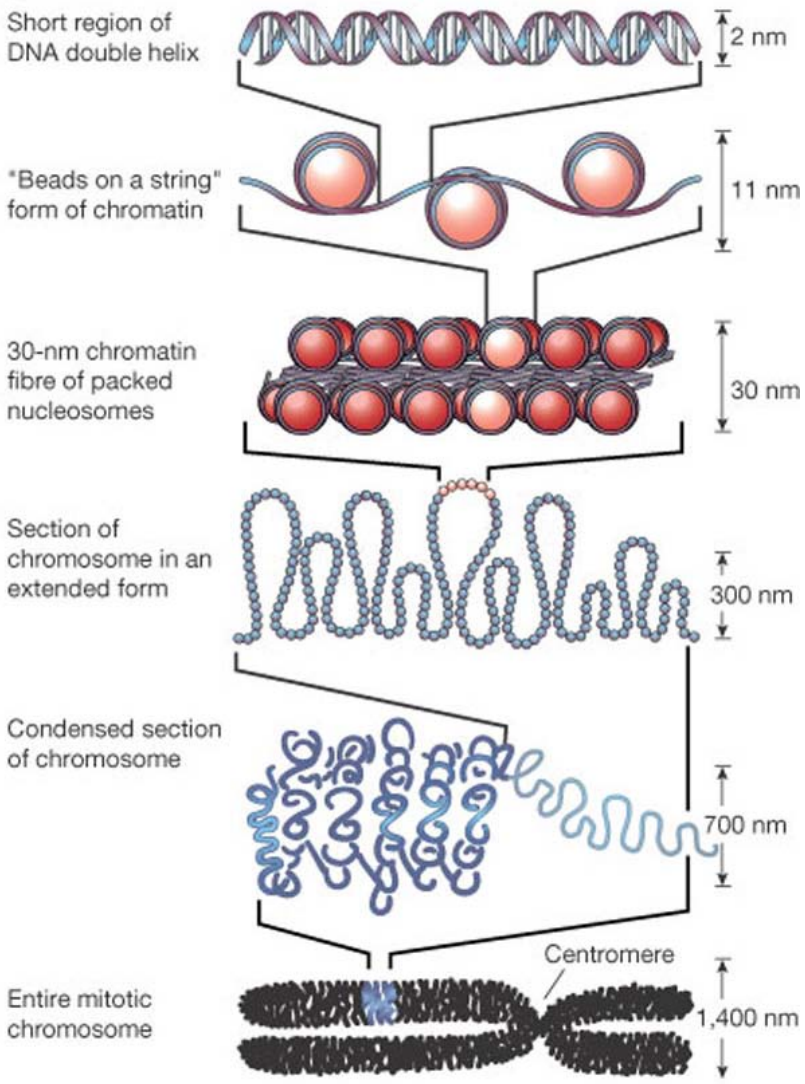

Fig. 1-1: Hierarchy of DNA organization inside a eukaryotic cell nucleus. Starting from the double helix, DNA is compacted into nucleosomes. The nucleosomes are then arranged in a “beads on a string” fashion and are further folded to form 30nm fibres. The fibres undergo further levels of compaction to lead to the chromosome. Reprinted from[11] with permission.

conformational dynamics. Previous work from the Widom lab showed that the nucleosomal DNA is in equilibrium between a wrapped and unwrapped conformations. This model is known as the "site-exposure" model[13-15]. The physiological reasoning behind this model is that DNA is often accessed by various proteins during replication, transcription, DNA repair and other cellular processes. If these "target" DNA sites are buried within the nucleosomes, they are sterically occluded and the bulky protein machinery will not be able to access these target sites[16]. To facilitate these cellular processes, DNA unwraps itself from the nucleosome and exposes itself while the opportunistic protein machinery binds to its target. This unwrapped state is short lived (few ms); however it is long enough for the binding events to happen. If no binding occurs within the time the DNA is unwrapped, the DNA rewraps back onto the protein core. Traditional biochemical assays like restriction enzyme accessibility were used to study this dynamics and establish the equilibrium constant for this process[17]. The results showed that the equilibrium constant for the site exposure is highest for DNA sites close to the exit from the nucleosomes while it decreases along the length of the DNA for the internal sites. This implies that the sites close to the exit are more accessible for proteins to act on them. Experiments done with stop-flow measurements and FRET combined with FCS showed that DNA within the nucleosome unwraps for approximately 10-50 ms before it rewraps. It then remains fully wrapped for about 250ms before it is unwraps again[13]. This

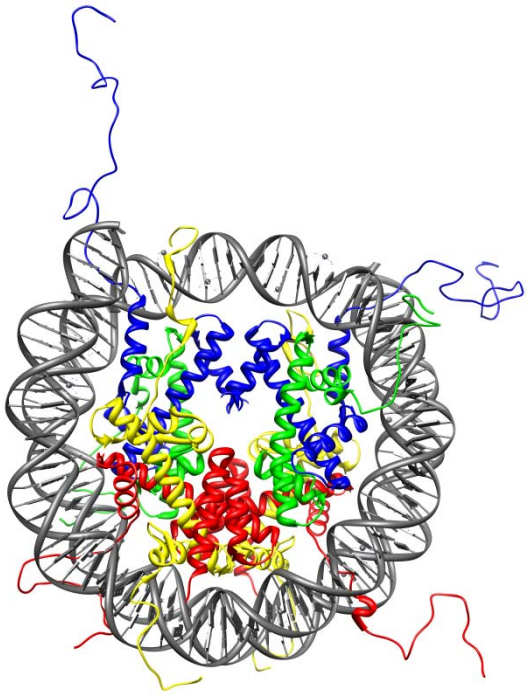

Fig. 1-2: Crystal structure of the nucleosome. Double helical DNA (in grey) is wrapped around a protein octamer core consisting of two copies each of histone proteins H2A (yellow), H2B (red),H3 (blue) and H4 (green). PDB file 1kx5[4] was used to generate this figure.

spontaneous unwrapping and rewrapping events helps the DNA binding proteins to find and associate to their target sites in a crowded chromatin environment. Fig. 1-3 shows a cartoon depiction of the "site exposure" model.

Other models of nucleosome dynamics includes both spontaneous conformational changes like nucleosome sliding (repositioning)[18,19] and induced conformational changes driven by chromatin remodeling enzymes which do so at the expense of ATP hydrolysis[20-23]. While the thermal repositioning dynamics are slower, the remodeling enzymes aid in the displacement of histones from the nucleosome and provide proteins with access to DNA[24]. These models work by regulating the position or density of nucleosomes along the genomic DNA.

Understanding the nature of the conformational dynamics is fundamental to understand gene regulation. These nucleosomes are substrates for any physiological process involving the DNA inside the nucleus of the cell. The states of wrapped and unwrapped DNA govern the transcription regulation.

Nucleosome assembly/disassembly

Nucleosomes present a barrier to various cellular processes. Various studies have shown that processes like transcription are slower *in vitro* when performed on reconstituted nucleosomes. These rates are slower compared to naked DNA *in vitro* and compared to *in vivo* rates[25]. Nucleosome disassembly has been shown to occur to increase the efficiency of these processes[26]. Disassembly includes removal of the H2A-H2B dimers from the octamer core followed by

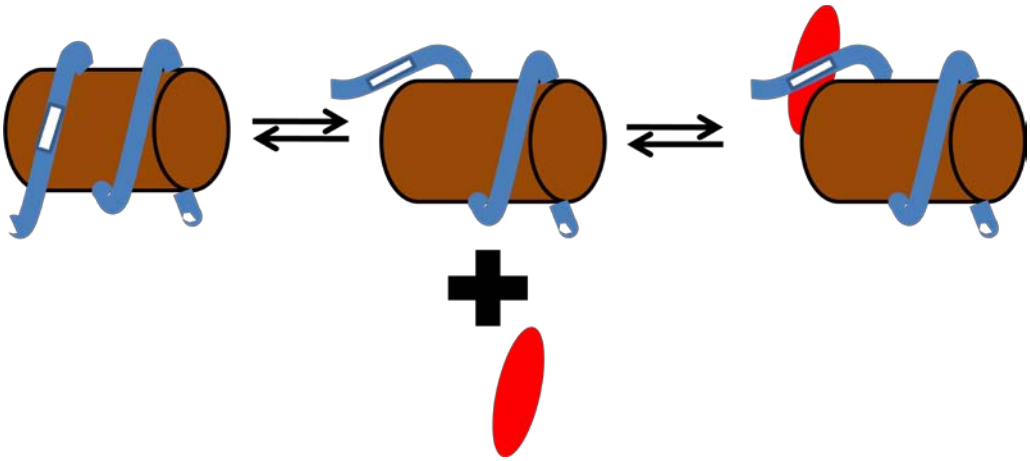

Fig. 1-3: Nucleosome Site Exposure model. Target DNA sequences (white) are exposed by transient unwrapping of the DNA (blue) from the octamer core (brown) and regulatory proteins (red) opportunistically bind to the exposed target sites.

removal of the $(H3\text{-}H4)_2$ tetramer. An intermediate in this process is by the replacement of major histones with their variants, thereby affecting nucleosome structure and function[27]. In fact, it has been shown that a transcriptionally active chromatin is depleted in (H2A-H2B) dimers[28]. However, the disassembly of the proteins has to be followed by re-assembly of the proteins to enable proper packaging of the DNA into chromatin. Discovering the pathway of nucleosome assembly and disassembly and recognition of the intermediates involved is very critical to understanding gene regulation.

Nucleosome assembly inside the cell requires the cooperative effort of various chromatin assembly factors and charperone proteins. In the cell, histone deposition is controlled by histone chaperones such as CAF-1, RCAF and NAP-1[27,29]. However when attempted to mix directly *in vitro* at physiological conditions, histones and DNA form insoluble non-nucleosomal aggregates. The chaperone proteins (which are rich in acidic residues) bind to the free histones and lead a pathway that prevents the whole octamer from immaturely binding to DNA. This assembly pathway must work in parallel to other cellular process like replication, DNA repair and transcription. Although there are clues to understand the mechanisms by which the chaperones assist the histone assembly, there is no direct evidence to prove them.

In vitro, nucleosome assembly is achieved in a sequential manner by lowering the ionic strength[30]. The buffer salt composition modulates the

electrostatic interactions of the nucleosome and has been used to mimic the activity of various factors *in vivo*. Briefly, the histone proteins and the DNA are placed in a high ionic strength solution (~2M NaCl) where the individual particles don't interact. The solution is slowly dialyzed against lower ionic strength solutions. The $(H3\text{-}H4)_2$ forms first and binds to the DNA at higher ionic strengths compared to the H2A-H2B dimer. This protocol does render some of the histone chaperone machinery redundant. This pathway is also assumed to be the one occurring *in vivo*.

Nucleosome disassembly is an important step to overcome the barrier posed by the nucleosomes to the protein machineries. Disassembly, like nucleosome assembly, is facilitated by chaperones and remodeling factors. Remodeling factors has been shown to facilitate binding between RNA polymerase and promoter DNA sequences[31]. While there are no studies to directly monitor nucleosome disassembly *in vivo*, a few studies have been undertaken to follow nucleosome disassembly *in vitro*. Salt assisted nucleosome disassembly has been used to mimic chaperone assisted nucleosome disassembly. The exact mechanism by which salt induces nucleosome disassembly is still unknown[32]. While some models predict that the whole octamer comes off in one step; others predict that disassembly following same pathway as assembly i.e. release of the H2A-H2B dimers first at lower salt concentration, followed by release of the H3-H4 tetramer.

In this work, we studied nucleosome dynamics through "site-exposure" model and salt assisted nucleosome disassembly with the use of fluorescent dyes that were positioned at appropriate labeling sites. The rest of this chapter is a brief introduction to the fluorescence techniques used in the thesis and a review of results obtained by other groups pursuing a similar approach to study nucleosomes.

Fluorescence Correlation Spectroscopy

Fluorescence Correlation Spectroscopy (FCS) is a powerful technique that correlates the stochastic fluctuations in fluorescence intensity within a very small detection volume (on the order of femtoliters). Since its inception in 1972, this technique has been extensively used in various biological applications[33,34]. Although the concept of FCS was formalized and experimentally demonstrated in early 1970s[35-37], the initial applications were restricted to large detection volume systems which lead to long experiments to obtain acceptable signal to noise ratios and statistical averages. However, over the last 15 years, advances in optics and high numerical aperture confocal microscopy have reduced the detection volume to less than a femtoliter. By using very dilute conditions (picomolar to nanomolar concentrations), only few molecules (0.1 to 100 on an average) are present in the confocal volume at any given time.

Fluorescence intensity arising from the few molecules is collected with high temporal resolution and the fluctuations from the mean intensities are

calculated. The fluctuations in fluorescence intensities are correlated and fitted with appropriate physical models to obtain information about physical processes that lead to these fluctuations. These processes include diffusion of the fluorescent molecule (translational and rotational), photochemical and photophysical reactions and conformational dynamics. The processes can occur as fast as a few picoseconds as for photon antibunching due to excitation-emission cycling[38], or as slow as seconds, as in the very slow 2D diffusion of membrane bound proteins. Most of FCS applications focus on studying diffusion rates of free fluorophores or fluorescenct-tagged target biomolecules, be it 3-dimensional, 2-dimensional, or anomalous diffusion[33,39-41]. FCS has also been applied to study conformational changes[13,42,43].

The application of FCS to study conformational dynamics in biomolecules is limited when attempted to measure dynamics slower than the diffusion of the molecules in the observation volume. The timescale of diffusion depends on the geometry of the observation volume and diffusion constant of the molecule. Attempts to study processes slower than diffusion have resulted in high noise levels. Alternatively attempts have been made to slow down diffusion by various mechanisms to increase the diffusion time and hence recover slower kinetic timescales.

FCS Principle

FCS is a statistical method based on analysis of fluorescence fluctuations. Typically, FCS experiments are performed on fluorescent dyes (and dye labeled molecules) that undergo Brownian motion. FCS instrumentation uses confocal microscopy (shown in Fig. 1-6) where a small observation volume is created. As the molecules diffuse in and out of the observation volume, fluctuations in the fluorescence intensity arise. Fluctuations in fluorescence intensity are defined as the deviation from the average intensity. It is described as:

$$\delta I(t) = I(t) - \langle I(t) \rangle \qquad 1\text{-}1$$

where $I(t)$ is the fluorescence intensity at any given time and $\langle I(t) \rangle$ is the mean fluorescence intensity over time. Fig. 1-4 shows a typical fluorescence intensity trace ($I(t)$). Fluctuations about the mean intensity, $\langle I(t) \rangle$, are then calculated.

Autocorrelation analysis is then performed on the fluctuation signal to recover the time structure of processes leading to the fluctuations. The autocorrelation function converts the fluctuations in the experiment time domain to correlation time domain to determine how long the fluctuations last.

To calculate the autocorrelation function, one compares the measured data with a time-shifted version (the lag time τ) of itself. If there is no time-shift, both data traces are identical - the correlation is high. If the shift is large, the two traces

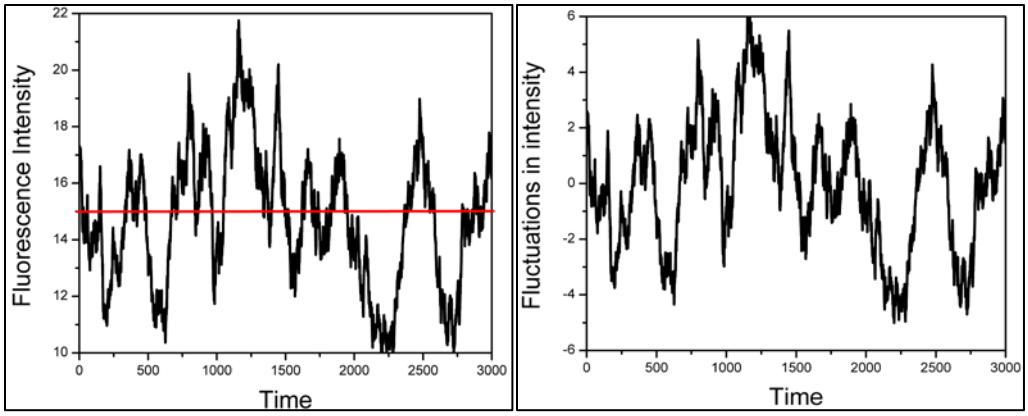

Fig. 1-4: Fluorescence intensity $I(t)$ is measured as a function of time. This is shown on the left. The mean intensity $\langle I(t) \rangle$ (shown in red) is then calculated and the fluctuations about the mean are calculated according to Eq. 1-1. The fluctuations are plotted as a function of time on the right. Note that the fluctuations average to zero, the midpoint of the y-axis on the right.

are very different - the correlation is low (this is true as long as the signal has no periodicity).

The normalized autocorrelation function is then calculated according to:

$$G(\tau) = \frac{\langle \delta I(t) \cdot \delta I(t+\tau) \rangle}{\langle I(t) \rangle^2} \quad \text{1-2}$$

where τ is the lag time and the autocorrelation function is normalized by the square of the mean intensity. Thus the autocorrelation function extracts timescales that give rise to the fluctuations. It serves as a "memory" function, to measure how long a signal stays similar.

The analytical expression for the autocorrelation functions for a single population of fluorophores (or fluorophore tagged molecules) undergoing translational diffusion in a three-dimensional Gaussian observation volume has been solved. It can be described in terms of the diffusion coefficient of the fluorophore, the dimensions of the confocal volume and the average number of fluorescent molecules as

$$G(\tau) = \frac{1}{\langle N \rangle} \cdot \frac{1}{1 + \frac{4D\tau}{r_0^2}} \cdot \frac{1}{\sqrt{1 + \frac{4D\tau}{z_0^2}}} \quad \text{1-3}$$

where D is the diffusion coefficient of the fluorophore, $\langle N \rangle$ is the mean number of molecules inside the confocal volume and r_0 and z_0 are the radial and axial axes of the confocal volume, shown in Fig. 1-6. The experimental

autocorrelation function for a freely diffusing tetramethyl rhodamine dye is shown in Fig. 1-5. It has been fitted according to Eq. 1-3.

The mean number of molecules is related to confocal volume (V) and the concentration of the fluorophore (C) and is given by

$$\langle N \rangle = C \cdot V \qquad 1\text{-}4$$

The confocal volume is related to the dimensions of the confocal volume by the following equation:

$$V = \pi^{3/2} \cdot r_0^2 \cdot z_0 \qquad 1\text{-}5$$

Any competing process that occurs at rates faster or comparable to diffusion timescale alters the fluorescence intensity and contributes to the autocorrelation function. For a system involving processes conformational dynamics that give rise to fluorescence fluctuations, the autocorrelation function is modified as

$$G_{total}(\tau) = G_{total}(\tau) \cdot X_{kinetic}(\tau) \qquad 1\text{-}6$$

where $X_{kinetic}(\tau)$ are the contributions from triplet dynamics and kinetics described as

$$X_{kinetic}(\tau) = 1 + \frac{1}{K_{eq}} \cdot e^{-(k_1+k_2)\cdot\tau} \qquad 1\text{-}7$$

where K_T and K_{eq} are the equilibrium constants for the processes and $\tau_{triplet}$ is the triplet time constant while k_1 and k_2 are the forward and backward rate constants for the kinetic reactions.

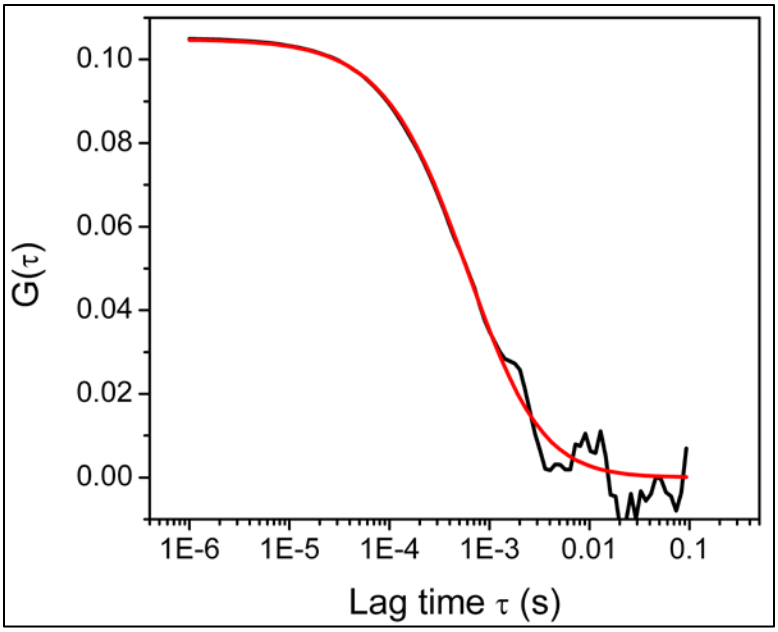

Fig. 1-5: Experimental autocorrelation function $G(\tau)$ obtained on freely diffusing tetramethyl rhodamine fluorescent dye. The autocorrelation is then fitted according to Eq. 1-3.

FCS instrumentation

FCS measurements are typically performed in a microscope with an optically restricted observation volume (confocal volume). This restriction of the detection to a small volume (few femtoliters) can be achieved in two ways. By using a pinhole in the image plane, out-of-focus fluorescence is eliminated and only fluorescence from the focal plane of the objective is detected. Another way to create confocal detection is by the use of two-photon illumination. The low probability of near-simultaneous absorption of two photons restricts the excitation profile. In this case, there is no need for a pinhole to reject out of focus light.

Förster Resonance Energy Transfer

To study conformational dynamics, FCS is often coupled with another popular fluorescence technique namely FRET (Förster Resonance Energy Transfer). In FRET, the molecule of interest is tagged with two spectrally distinguishable fluorophores (donor and acceptor). The fluorophores are chosen such that there is spectral overlap between the fluorescence emission spectrum of the donor and the absorption spectrum of the acceptor. The donor is excited to its first excited electronic state through the use of a suitable light source. The energy of the excited state is then transferred to an acceptor fluorophore when the acceptor, if the acceptor molecule is in the vicinity of the donor molecule. The efficiency of energy transfer is described as the quantum yield of the energy

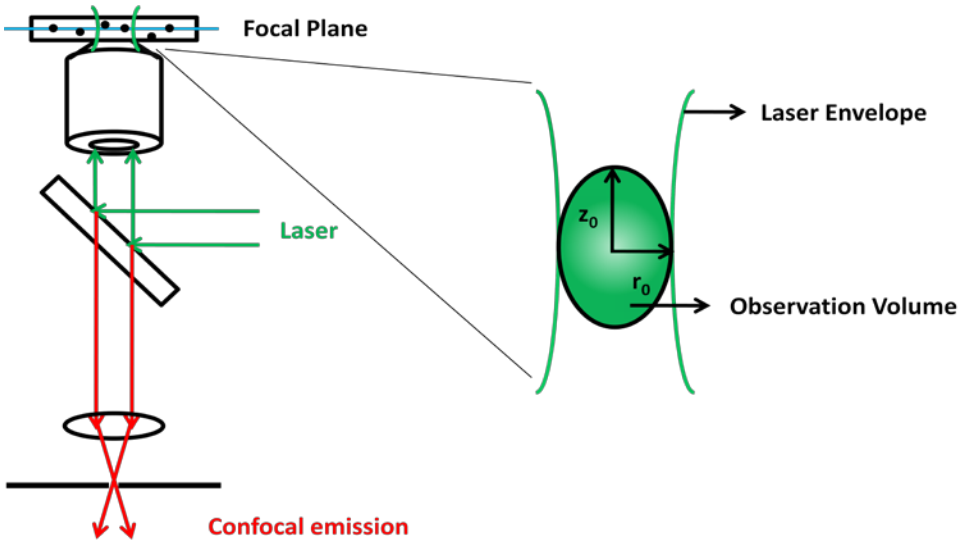

Fig. 1-6: Principle of confocal microscopy. A high numerical aperture (NA) objective focuses the laser to create a tight laser envelope. Use of a pinhole with a small aperture (~10-100 µm) at a location confocal to the focal plane rejects out of focus light and allows emission from the focal plane only (confocal emission). The resulting optically restricted volume is shown on the right. The confocal volume is a 3-dimensional volume with the intensity decreasing as a Gaussian function along x-y plane with a $1/e^2$ radius of r_0 and the intensity decreasing as a Gaussian function along the z-axis with a $1/e^2$ radius of z_0.

transfer *i.e.* the fraction of energy transfer event occurring per donor excitation event:

$$E = \frac{k_{ET}}{k_f + k_{ET} + \sum k_i} \quad \text{1-8}$$

where k_{ET} is the rate of energy transfer, k_f is the radiative decay rate of the donor and k_i(s) are the rate constants of other pathways that compete with fluorescence to de-excite the electrons in the excited state. A simplified Jablonski diagram to represent FRET is shown in Fig. 1-7.

This non-radiative transfer of energy occurs via dipole-dipole coupling. The efficiency of this energy transfer is distance dependent given by

$$E = \frac{R_0^6}{R_0^6 + r^6} \quad \text{1-9}$$

and hence can be used as a technique to measure the distance between the two fluorophores. Here, r is the distance between the two fluorophores and R_0 is the Förster distance for the donor-acceptor couple. Fig. 1-8 shows the dependence of FRET efficiency (E) on the distance between the fluorophores (r). The Förster distance depends on the spectral overlap between the fluorescence emission of the donor and the fluorescence excitation of the acceptor, the fluorescence quantum yield of the donor and the relative orientation between the fluorophores. The typical Förster distance for commonly used FRET pairs is around 50Å and hence FRET is used to measure distance in the 10-100Å range. To study conformational

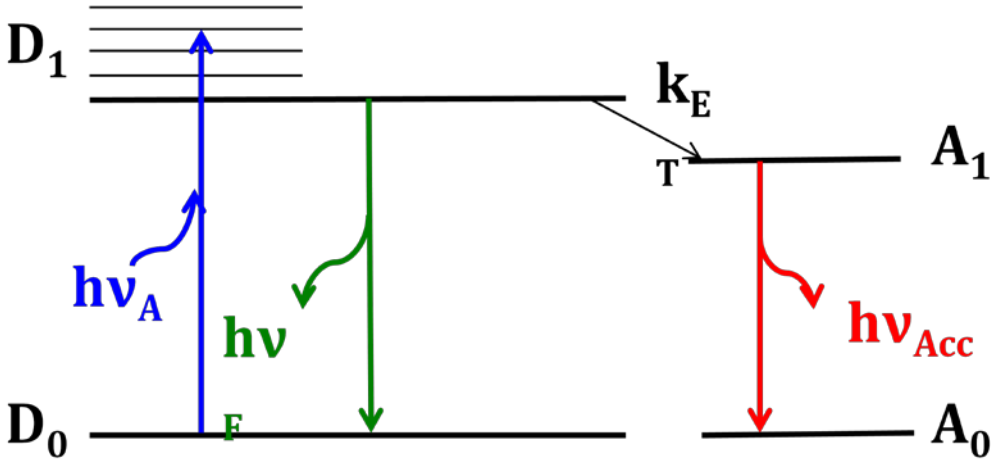

Fig. 1-7: Simplified Jablonski diagram representing FRET. A donor fluorophore in its ground electronic state (S_0) is excited with an appropriate light source (energy $E = h\nu_A$). From the excited electron state (S_1), the electron can be de-excited back to the ground state through multiple pathways: by emitting a fluorescent photon (energy $E = h\nu_f$) with a rate of k_f^{Donor} or by transferring the energy non-radiatively to an adjacent acceptor fluorophore. The acceptor fluorophore thus emits a fluorescent photon (energy $E = h\nu_{Acc}$).

dynamics, the FRET donor and acceptor fluorophores are attached to the molecule(s) of interest such that there is a significant change in FRET efficiency while the molecule is undergoing conformational dynamics. FRET was first proposed in 1948 by Förster[44] and was pioneered by Stryer[45] who used the term "spectroscopic ruler" to describe FRET.

Originally FRET experiments were performed on large number of molecules ("bulk" FRET measurements). However, it was recently demonstrated that FRET experiments can be performed at a single molecule level. Single molecule FRET (smFRET)[46] has revolutionized the field of biophysics by offering multiple advantages over the bulk measurements. The ability to detect the presence of sub-populations within a heterogeneous sample and measuring dynamic information are some of the advantages of smFRET. smFRET experiments are either done on molecules freely diffusing in solution by use of confocal microscopy or by immobilizing the molecule on a surface and studying them using total internal reflection fluorescence microscopy (TIRFM)[47]. smFRET have been used to study structural changes in nucleic acids and proteins[46,48-50].

Experimental determination of FRET efficiency *E* can be done in multiple ways. In a bulk FRET assay, the fluorescence emission spectrum of the sample is recorded by illuminating the sample at a wavelength where the donor absorbs. Depending on the FRET efficiency of the molecule, the peaks of the donor (and acceptor) emission increase (and decrease) as shown in Fig. 1-9.

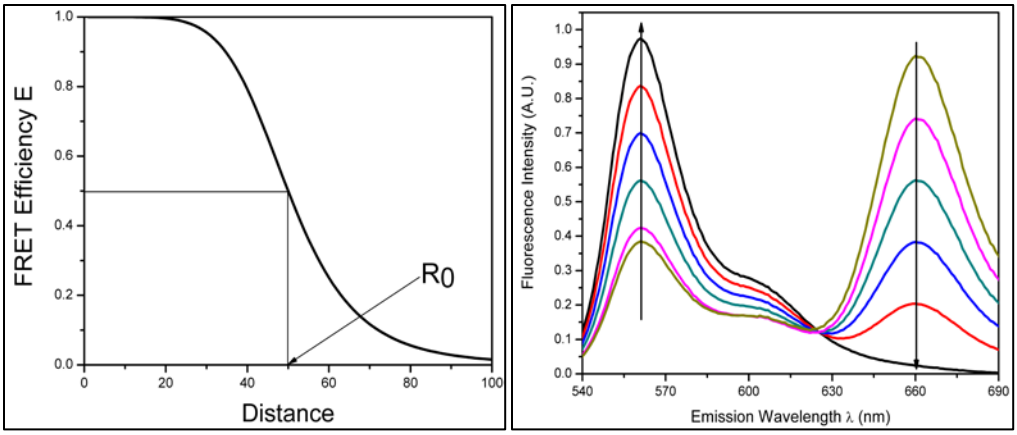

Fig. 1-8 (left): FRET efficiency vs. distance plot. The sixth power dependence of FRET efficiency on distance between the FRET donor and acceptor makes it a very suitable technique to sense distance changes especially around the Förster distance R_o.

Fig. 1-9 (right): Fluorescence Emission Spectrum from a FRET sample. The sample is excited at a wavelength where the donor absorbs and the fluorescence emission of both the donor and the acceptor are recorded. As the FRET efficiency of the sample decreases, the emission from the acceptor decreases and the emission from donor increases. The trends are indicated by the arrows.

FCS and FRET have been combined to study conformational dynamics of biomolecules[13,42,43]. As the molecules undergo conformational dynamics, the distance between the donor and the acceptor changes. This results in fluctuations in the FRET efficiency. The fluctuations are also observed as fluctuations in the intensities of the donor and acceptor and hence the timescales can be recovered using correlation analysis. In these experiments involving FRET and FCS, two detectors are used to measure the fluorescence intensities of the FRET donor and FRET acceptor and the intensities measured in either detector can be autocorrelated with itself and they can also be correlated against each other resulting in an a crosscorrelation function. The crosscorrelation function is defined as

$$G_{cross}(\tau) = \frac{\langle \delta I_1(t) \cdot \delta I_2(t+\tau) \rangle}{\langle I_1(t) \rangle \cdot \langle I_2(t) \rangle} \qquad 1-10$$

where I_1 and I_2 are the intensities measured in channel 1 and 2 and $\langle I_1(t) \rangle$ and $\langle I_2(t) \rangle$ are the mean intensities in the respective channels.

Single Molecule Fluorescence experiments on nucleosomes

Nucleosome dynamics using Fluorescence Correlation Spectroscopy

Fluorescence Correlation Spectroscopy (FCS) has been used to study nucleosome dynamics at a few-molecule level. FCS studies were done on freely diffusing nucleosomes which offer a huge advantage compared to immobilizing nucleosomes on surfaces to perform single-molecule FRET experiments. Previous

studies have shown that a high fraction of nucleosomes are not stable and fall apart upon immobilization[51]. FCS can also access timescales much shorter than single molecule FRET experiments. FCS combined with FRET revealed nucleosome dynamics and established the kinetic rates of "site-exposure" model[13]. A slight variation of the method was used to confirm the original results. Instead of using a separate donor only control[13] which could lead to introduction of artifacts due to changes in observation volume, Torres and Levitus used an approach where the correlation curves are obtained from a single double-labeled sample[52]. The results obtained in this study agreed with previous results. Role of various DNA sequences on nucleosome dynamics was studied using FCS by Kelbauskas *et al*. Sequences explored were naturally occurring sequences including a TATA-containing sequence from the yeast GAL10 promoter, a regulatory sequence from the MMTV promoter, and a fragment from the well-studied sea urchin 5S rDNA gene[53,54]. Significant differences were observed between the 5S nucleosome and the two promoter sequence nucleosomes indicating direct evidence between nucleosome dynamics and transcription regulation. Koopmans *et al.* performed FCS on subpopulations of nucleosomes and showed that even under various conformation of nucleosome, there exists equilibrium between unwrapped and rewrapped states[55]. Burst analysis was performed to select nucleosome subpopulations and FCS was performed on selected bursts and the diffusion times of each subpopulation were reported.

Böhm et al. used FCS to study salt induced conformational changes in nucleosomes and showed that the salt induced disassembly is a multi-step pathway[32]. Their results support the mechanism where the H2A-H2B dimer first disassociates from the nucleosome core followed by the $(H3\text{-}H4)_2$ tetramer instead of the mechanism where the whole histone octamer is removed in one step. They were also able to probe a previously unknown intermediate where the DNA unwraps and the H2A-H2B dimer peels off from the protein core but is still in contact with the tetramer as shown in Fig 1-10.

Single Molecule FRET experiments on immobilized nucleosomes

Nucleosome dynamics was measured on immobilized nucleosomes using TIRF microscopy and reported by Tomchik *et al*.[56]. In this work, 164-bp DNA GUB nucleosome positioning sequence was used which was labeled with the FRET pair Cy3 and Cy5 and was tethered to the surface using biotin-streptavidin chemistry. The fluorescent dyes were attached covalently to amino-modifed bases located on opposite strands so that their final location on the double helix was equidistant from the nucleosome dyad, and 75 bp apart from each other. This distance is more than four times the Förster distance for this FRET pair, and therefore the efficiency of FRET is expected to be negligible unless the two dyes are brought close together by the interaction between the DNA and the histones. The reconstitution of the nucleosome results in a distance of 3nm between the

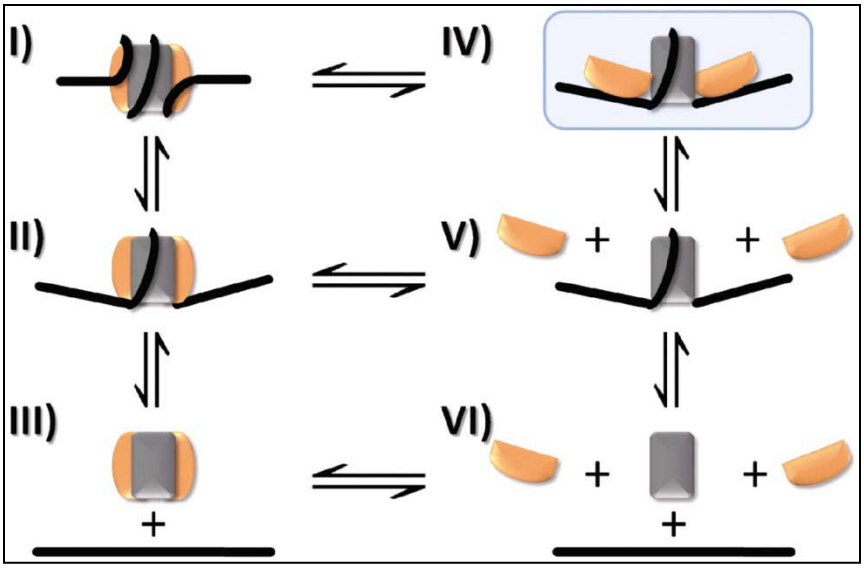

Fig 1-10: Intermediates in the nucleosome disassembly pathway. Using FCS to find the diffusion coefficients of individual disassembly products, Böhm et al.[32] connected the dots between a complete intact nucleosome (I) and complete disassembly (VI). Intermediate II is the product of "site-exposure". State IV (shaded in blue) was a previously unknown intermediate, detected in this study. Reprinted with permission.

fluorophores resulting in high FRET. Therefore, changes in FRET efficiency between a high- and a low- value are expected to be indicative of wrapping-unwrapping transitions. Using this approach, the authors observed long-range DNA breathing of more than 35bp which they referred to as 'opening'. The reported mean lifetimes were 2-5 seconds in the wrapped conformation and 100-250 ms in the unwrapped conformation depending on ionic strength. These results were an order of magnitude away from the times reported by Li *et al*[13]. A later study by Koopmans *et al.* used alternate laser excitation (ALEX) and demonstrated that most of the apparent FRET transitions reported in this paper were not due to nucleosomal dynamics, but due to acceptor photophysics[57]. A re-investigation of the method and results by the former group also concluded that most of the FRET "transitions" were due to photoblinking of the acceptor A later study by Koopmans *et al.* used alternate laser excitation (ALEX) and demonstrated that most of the apparent FRET transitions reported in this paper were not due to nucleosomal dynamics, but to acceptor photophysics[58]. In other words, most of the events that led to a decrease in Cy5 fluorescence intensity (and concomitant increase in Cy3 intensity) were of photophysical origin, and had been erroneously interpreted as changes in nucleosome conformation. Both study showed that it is important to address acceptor blinking by use of Trolox[59], a water soluble derivative of vitamin E. As an antioxidant, like vitamin E, it is used to suppress the oxidation of acceptor and thus reduce its blinking. Immobilization

of nucleosomes also leads to disintegration of nucleosomes. In the work by Koopmans *et al.*[57] used nucleosomes prepared from recombinant histone octamers and a 177 bp DNA construct based on the 601 nucleosome positioning sequence developed by the Widom lab[60]. The study reported that only 10% of the nucleosomes appeared as intact complexes, and 97% of the intact nucleosomes did not show any significant change in FRET during the accessible observation time (10 ms-10's of seconds). Despite surface passivation with polyethylene glycol (PEG), only 3% of the intact nucleosomes showed FRET fluctuations related to nucleosome dynamics. In a subsequent study by the same group[51], nucleosome stability was studied with respect to immobilization techniques with the goal of studying surface artifacts and finding appropriate surface for nucleosome studies. The different surfaces studies were BSA, PEG and starPEG (6-arm PEG that forms cross-links). The conclusion of this work is that the star PEG coating performs yields the best surface in terms of nucleosome integrity. StarPEG coating prevented nonspecific tethering most effectively and reported lifetimes of nucleosome dynamics that were in good agreement with the times reported by Li *et al.* [13].

Single molecule FRET experiments on diffusing nucleosomes

Gansen *et al.* performed smFRET experiments on freely diffusing nucleosomes and investigated the influence of salt concentration, nucleosome concentration and crowding agents on nucleosome stability[61]. With sample

concentrations downs to ~40 pM (effective average of 0.03 molecules in the observation volume at any given time), dye photophysics and nucleosome stability were studied. They showed that crowding agents like BSA (at 0.2 mg/ml concentration) helps in maintaining nucleosome integrity even at 300mM NaCl. They also claim that BSA is superior to unlabeled nucleosomes which have been used as crowding agents to stabilize nucleosomes under single molecule conditions. Studies by the same group demonstrated using smFRET that histone acetylation decreases nucleosome stability[62]. This is the first measurement on effect of histone acetylation on nucleosome structure. A more quantitative analysis of FRET histograms of freely diffusing mononucleosomes was performed by the same group[63]. Multiparameter fluorescence detection was performed along with probability distribution analysis (PDA) to measure the FRET efficiencies, fluorescence lifetimes and fluorescence anisotropy of nucleosome subpopulations. The results revealed at least four different subspecies with different FRET efficiency: three nucleosome species, with high (~0.5), medium, (~0.32) or low (close to zero) FRET, and a donor-only population. Salt dependent stability analysis of these species identified these populations as intermediates in nucleosome disassembly. Based on these observations, a model is proposed for stepwise dissociation: first unwrapping from the ends, than dimer loss, and finally complete dissociation.

Scope of this thesis

Equilibrium constants for accessibility of DNA at various sites, from the end of the DNA to sites near the dyad axis, were measured using biochemical techniques. Results showed that the equilibrium constants progressively decreased from ends towards the middle[17,64,65]. While the equilibrium constants only provide a static picture, our goal is recover the kinetic rate constants of the nucleosome dynamics at sites near the end of the DNA to sites near the middle of the DNA. We used a FRET based system and labeled the nucleosomes with a FRET donor and acceptor at suitable locations to recover the kinetics at these sites. Chapter 2 will describe the FRET system in detail and discuss the results obtained. The salt induced nucleosome disassembly has been studied using smFRET; however the experimental conditions used in the studies promote nucleosome disintegration and the results may not reflect the actual process. Use of dual color crosscorrelation to identify the presence of doubly labeled samples will avoid the necessity to work in dilute conditions thus maintain nucleosome stability. Chapter 3 will describe the use of FRET fluctuation spectroscopy towards conformational dynamics focusing on its applicability for nucleosome dynamics. Chapter 4 will discuss the work done on dual color crosscorrelation spectroscopy to study salt-assisted nucleosome disassembly.

Reference

(1) Kornberg, R. D. *Annu. Rev. Biochem* **1977**, *46*, 931-954.

(2) Kornberg, R. D. *Science* **1974**, *184*, 868-871.

(3) Kornberg, R. D.; Thomas, J. O. *Science* **1974**, *184*, 865-868.

(4) Davey, C. A.; Sargent, D. F.; Luger, K.; Maeder, A. W.; Richmond, T. J. *J. Mol. Biol.* **2002**, *319*, 1097-1113.

(5) Luger, K.; Rechsteiner, T. J.; Flaus, A. J.; Waye, M. M. Y.; Richmond, T. J. *J. Mol. Biol.* **1997**, *272*, 301-311.

(6) Segal, E.; Fondufe-Mittendorf, Y.; Chen, L. Y.; Thastrom, A.; Field, Y.; Moore, I. K.; Wang, J. P. Z.; Widom, J. *Nature* **2006**, *442*, 772-778.

(7) Yager, T. D.; Mcmurray, C. T.; Vanholde, K. E. *Biochemistry* **1989**, *28*, 2271-2281.

(8) Mangenot, S.; Leforestier, A.; Vachette, P.; Durand, D.; Livolant, F. *Biophys. J.* **2002**, *82*, 345-356.

(9) Strahl, B. D.; Allis, C. D. *Nature* **2000**, *403*, 41-45.

(10) Allfrey, V. G.; Faulkner, R.; Mirsky, A. E. *Proc. Natl. Acad. Sci. USA* **1964**, *51*, 786-&.

(11) Felsenfeld, G.; Groudine, M. *Nature* **2003**, *421*, 448-453.

(12) Thoma, F.; Koller, T.; Klug, A. *J. Cell Biol.* **1979**, *83*, 403-427.

(13) Li, G.; Levitus, M.; Bustamante, C.; Widom, J. *Nat. Struct. Mol. Biol.* **2005**, *12*, 46-53.

(14) Li, G.; Widom, J. *Nat. Struct. Mol. Biol.* **2004**, *11*, 763-769.

(15) Anderson, J. D.; Thastrom, A.; Widom, J. *Mol. Cell. Biol.* **2002**, *22*, 7147-7157.

(16) Kornberg, R. D.; Lorch, Y. L. *Cell* **1999**, *98*, 285-294.

(17) Polach, K. J.; Widom, J. *J. Mol. Biol.* **1995**, *254*, 130-149.

(18) Flaus, A.; Owen-Hughes, T. *Mol. Cell. Biol.* **2003**, *23*, 7767-7779.

(19) Pennings, S.; Meersseman, G.; Bradbury, E. M. *J. Mol. Biol.* **1991**, *220*, 101-110.

(20) Teif, V. B.; Rippe, K. *Nucleic Acids Res.* **2009**, *37*, 5641-5655.

(21) Whitehouse, I.; Flaus, A.; Cairns, B. R.; White, M. F.; Workman, J. L.; Owen-Hughes, T. *Nature* **1999**, *400*, 784-787.

(22) Whitehouse, I.; Flaus, A.; Havas, K.; Owen-Hughes, T. *Biochem. Soc. Trans.* **2000**, *28*, 376-379.

(23) Varga-Weisz, P. D.; Becker, P. B. *Curr. Opin. Cell Biol.* **1998**, *10*, 346-353.

(24) Schiessel, H. *J. Phys.: Condens. Matter* **2003**, *15*, R699-R774.

(25) Izban, M. G.; Luse, D. S. *J. Biol. Chem.* **1992**, *267*, 13647-13655.

(26) Kireeva, M. L.; Hancock, B.; Cremona, G. H.; Walter, W.; Studitsky, V. M.; Kashlev, M. *Mol. Cell* **2005**, *18*, 97-108.

(27) Park, Y. J.; Dyer, P. N.; Tremethick, D. J.; Luger, K. *J. Biol. Chem.* **2004**, *279*, 24274-24282.

(28) Kireeva, M. L.; Walter, W.; Tchernajenko, V.; Bondarenko, V.; Kashlev, M.; Studitsky, V. M. *Mol. Cell* **2002**, *9*, 541-552.

(29) Akey, C. W.; Luger, K. *Curr. Opin. Struct. Biol.* **2003**, *13*, 6-14.

(30) Wilhelm, F. X.; Wilhelm, M. L.; Erard, M.; Daune, M. P. *Nucleic Acids Res.* **1978**, *5*, 505-521.

(31) Paranjape, S. M.; Kamakaka, R. T.; Kadonaga, J. T. *Annu. Rev. Biochem* **1994**, *63*, 265-297.

(32) Bohm, V.; Hieb, A. R.; Andrews, A. J.; Gansen, A.; Rocker, A.; Toth, K.; Luger, K.; Langowski, J. *Nucleic Acids Res.*

(33) Hess, S. T.; Huang, S.; Heikal, A. A.; Webb, W. W. *Biochemistry* **2002**, *41*, 697-705.

(34) Thompson, N. L.; Lieto, A. M.; Allen, N. W. *Curr Opin Struct Biol* **2002**, *12*, 634-41.

(35) Elson, E. L.; Magde, D. *Biopolymers* **1974**, *13*, 1-27.

(36) Magde, D.; Elson, E. L.; Webb, W. W. *Biopolymers* **1974**, *13*, 29-61.

(37) Magde, D.; Webb, W. W.; Elson, E. *Phys. Rev. Lett.* **1972**, *29*, 705-&.

(38) Lounis, B.; Bechtel, H. A.; Gerion, D.; Alivisatos, P.; Moerner, W. E. *Chem. Phys. Lett.* **2000**, *329*, 399-404.

(39) Fatin-Rouge, N.; Starchev, K.; Buffle, J. *Biophys. J.* **2004**, *86*, 2710-2719.

(40) Banks, D. S.; Fradin, C. *Biophys. J.* **2005**, *89*, 2960-2971.

(41) Sanabria, H.; Kubota, Y.; Waxham, M. N. *Biophys. J.* **2007**, *92*, 313-322.

(42) Eggeling, C.; Fries, J. R.; Brand, L.; Gunther, R.; Seidel, C. A. M. *Proc. Natl. Acad. Sci. USA* **1998**, *95*, 1556-1561.

(43) Bonnet, G.; Krichevsky, O.; Libchaber, A. *Proc. Natl. Acad. Sci. USA* **1998**, *95*, 8602-8606.

(44) Forster, T. *Annalen Der Physik* **1948**, *2*, 55-75.

(45) Stryer, L.; Haugland, R. P. *Proc. Natl. Acad. Sci. USA* **1967**, *58*, 719-&.

(46) Ha, T.; Enderle, T.; Ogletree, D. F.; Chemla, D. S.; Selvin, P. R.; Weiss, S. *Proc. Natl. Acad. Sci. USA* **1996**, *93*, 6264-6268.

(47) Ha, T. *Methods* **2001**, *25*, 78-86.

(48) Michalet, X.; Weiss, S.; Jager, M. *Chem. Rev.* **2006**, *106*, 1785-1813.

(49) Seidel, R.; Dekker, C. *Curr. Opin. Struct. Biol.* **2007**, *17*, 80-86.

(50) Zhuang, X. W. *Annu. Rev. Biophys. Biomol. Struct.* **2005**, *34*, 399-414.

(51) Koopmans, W. J. A.; Schmidt, T.; van Noort, J. *Chemphyschem* **2008**, *9*, 2002-2009.

(52) Torres, T.; Levitus, M. *J. Phys. Chem. B* **2007**, *111*, 7392-400.

(53) Kelbauskas, L.; Chan, N.; Bash, R.; DeBartolo, P.; Sun, J.; Woodbury, N.; Lohr, D. *Biophys. J.* **2008**, *94*, 147-158.

(54) Kelbauskas, L.; Chan, N.; Bash, R.; Yodh, J.; Woodbury, N.; Lohr, D. *Biochemistry* **2007**, *46*, 2239-2248.

(55) Koopmans, W. J. A.; Buning, R.; Schmidt, T.; van Noort, J. *Biophys. J.* **2009**, *97*, 195-204.

(56) Tomschik, M.; Zheng, H.; van Holde, K.; Zlatanova, J.; Leuba, S. H. *Proc Natl Acad Sci U S A* **2005**, *102*, 3278-83.

(57) Koopmans, W. J.; Brehm, A.; Logie, C.; Schmidt, T.; van Noort, J. *J Fluoresc* **2007**, *17*, 785-95.

(58) Tomschik, M.; van Holde, K.; Zlatanova, J. *J Fluoresc* **2009**, *19*, 53-62.

(59) Rasnik, I.; McKinney, S. A.; Ha, T. *Nat Methods* **2006**, *3*, 891-3.

(60) Lowary, P. T.; Widom, J. *J Mol Biol* **1998**, *276*, 19-42.

(61) Gansen, A.; Hauger, F.; Toth, K.; Langowski, J. *Anal Biochem* **2007**, *368*, 193-204.

(62) Gansen, A.; Toth, K.; Schwarz, N.; Langowski, J. *J. Phys. Chem. B* **2009**, *113*, 2604-13.

(63) Gansen, A.; Valeri, A.; Hauger, F.; Felekyan, S.; Kalinin, S.; Toth, K.; Langowski, J.; Seidel, C. A. *Proc Natl Acad Sci U S A* **2009**, *106*, 15308-13.

(64) Polach, K. J.; Widom, J. *J. Mol. Biol.* **1996**, *258*, 800-812.

(65) Polach, K. J.; Widom, J. *Chromatin* **1999**, *304*, 278-298.

Chapter 2

POSITION-DEPENDENT NUCLEOSOME SITE EXPOSURE KINETICS

Introduction

Eukaryotic DNA undergoes various cellular processes and is often targeted by bulky protein machineries to carry out replication, transcription and repair function. These protein systems can only act on naked DNA substrates and this requires the DNA target sites to peel off the histone proteins as the arrangement of DNA on nucleosomes sterically occludes the DNA[1]. The mechanism by which these enzyme complexes access their target sites is not clearly understood. Various models are used to represent the DNA conformational changes. One mechanism is the nucleosome remodeling complexes which utilize the chemical energy of ATP-hydrolysis to power the removal of DNA from the nucleosome[2,3]. However, this is an energy driven process and could be expensive for the cell[4]. This led to the hypothesis that nucleosomes, in spite of being a robust protein-DNA complex, are not static entities but instead are dynamic. This hypothesis assumes that DNA transiently unwraps from the nucleosome and is accessible to DNA binding proteins. Using standard biochemical assays, the Widom lab established that this hypothesis is true and stretches of DNA spontaneously yet transiently unwrap from the nucleosome starting from one end. This model is called the "site-exposure" model[5-8] and the equilibrium constant for this process has been established[5,9]. The

equilibrium constants indicate that near the end of the nucleosomal DNA, the DNA is unwrapped for 1-10% of the time. However, for DNA sites near the middle of dyad axis the equilibrium constant is as low as ~ 10^{-6} (Fig. 2-1). Other groups have provided further evidence to support this spontaneous nucleosomal site exposure by measuring the rate of RNA polymerase and other processive enzymes to traverse along a DNA reconstituted on a nucleosome[10]. *In vitro* studies carried out by Hodges[10] suggest that RNA polymerase II does not actively unwrap nucleosomes. Instead, it waits for these fluctuations spontaneous to occur and then uses the opportunity to bind to its target site. These studies show that the "site exposure" mechanism facilitates the cellular processes and allows proteins to bind to their target sites[11,12].

While equilibrium constants establish the population of nucleosomes in either the wrapped or unwrapped conformations, it fails to yield information on the kinetic rates of these processes. The intrinsic nucleosome dynamics can facilitate the DNA binding abilities of the regulatory proteins only if the lifetime of the unwrapped conformation is long enough for proteins to bind to them. Previous studies using stopped-flow measurements in conjunction with FRET-FCS measurements have established the rates for ends of nucleosomal DNA[8] (Fig. 2-2). The study showed that the DNA remains fully wrapped for ~ 250 milliseconds (corresponding rate of 4 s^{-1}) before spontaneously unwrapping. The unwrapped state, on an average, last ~20-50 milliseconds before re-wrapping

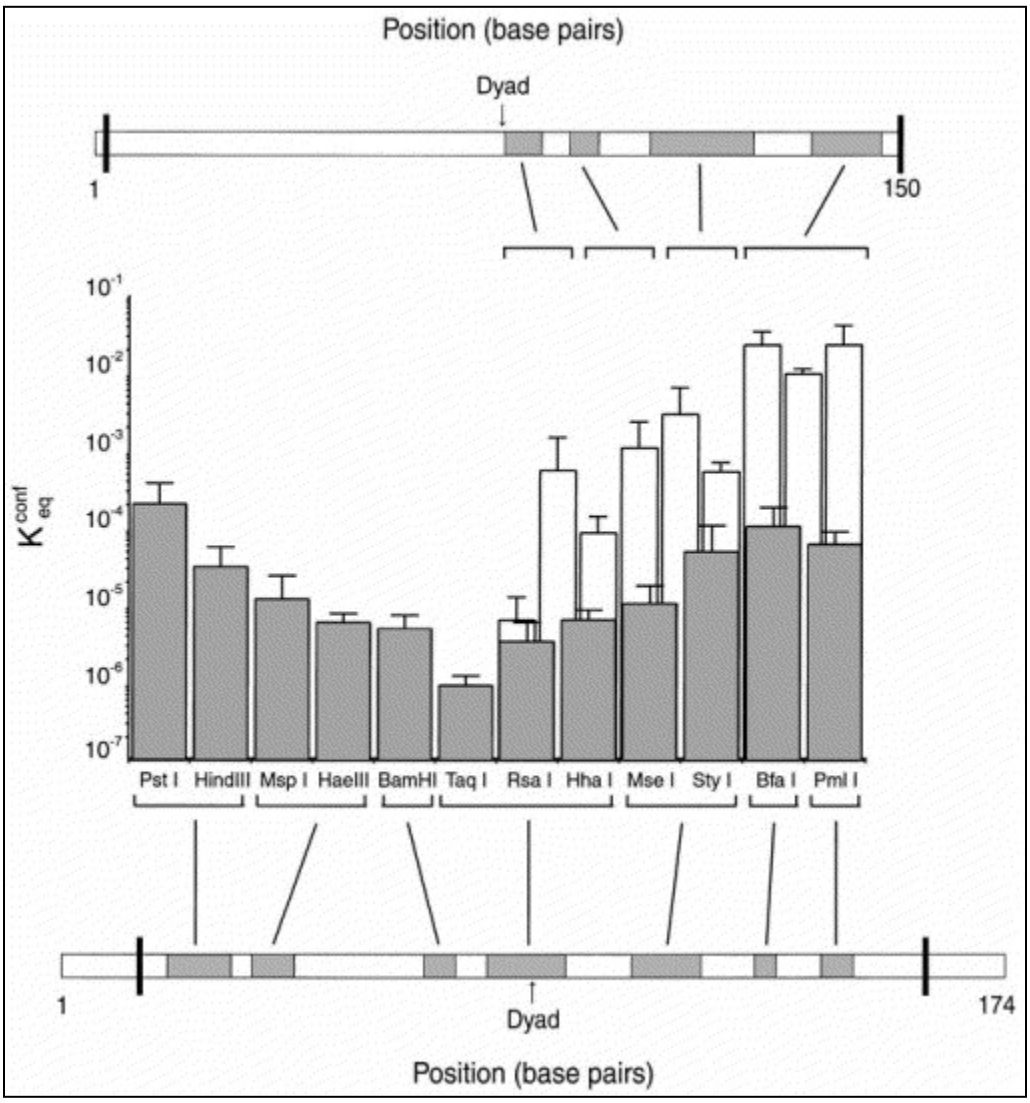

Fig. 2-1: Equilibrium constants measured for site exposure (K_{eq}) using the synthesized "601" nucleosome positioning sequence (dark shades) and a naturally occurring 5S sequence (white boxes)[9]. The accessibility to restriction was used to quantify the equilibrium constants. Reprinted with permission.

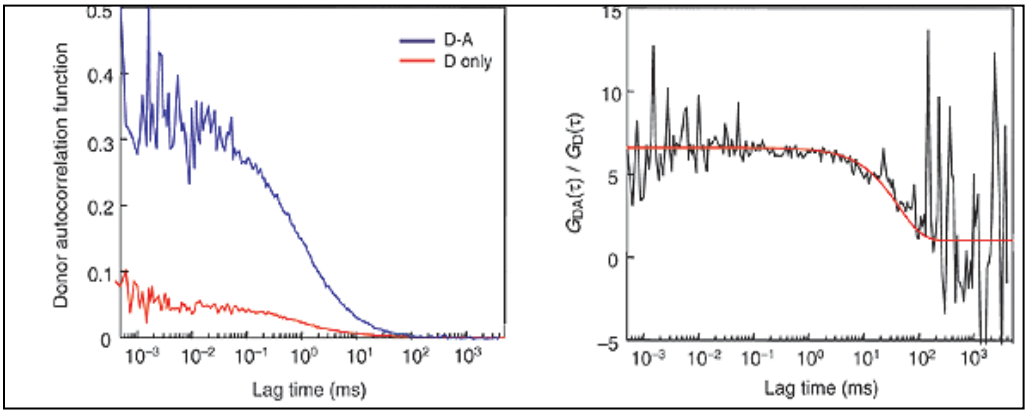

Fig. 2-2: FRET-FCS analysis to measure nucleosome dynamics at the end of the DNA[8]. The autocorrelation on donor intensity (left) were performed on the dual labeled sample (D-A) and on a control donor-only sample (D only). The ratio of the two autocorrelation was fitted to extract the kinetic information (right). Reprinted with permission.

(corresponding rate of 20-50 s^{-1}) yielding an equilibrium constant of 0.08-0.2 consistent with previous results. These timescales are physiologically significant as this is the time required for a regulatory protein to recognize and bind to target sites *in vivo*.

FCS has been applied to study conformational dynamics in nucleic acids and nucleic acid- protein complexes before. FCS experiments are typically performed in confocal observation volume (~ one femtoliter) and under dilute conditions (~picomolar to nanomolar concentrations) which give rise to an average of 1-100 molecules in the confocal volume at any given time. The temporal fluctuations in the fluorescence intensity are collected and analyzed statistically to yield timescales of processes leading to these fluctuations. These processes include concentration fluctuations via molecular diffusion, chemical reactions, photophysical processes, and so on. FCS has been used to measure the conformational dynamics of DNA hairpins[13-15], nucleosomes[8,16,17], breathing in double stranded DNA[18], DNA mobility and flexibility[19] and RNA recognition by proteins[20].

After the initial study to measure site-exposure nucleosome dynamics by Li et al., several other groups have attempted to study nucleosome dynamics using FCS. Kelbauskas et al. studied role of DNA sequence on nucleosome stability and dynamics using FRET-FCS. In this study, the authors used three sequences: a TATA-containing sequence from the yeast GAL10 promoter, a regulatory

sequence from the MMTV promoter, and a fragment from the well-studied sea urchin 5S rDNA gene[16,21]. While the former two sequences are transcriptionally active sequences, the third sequence was transcriptionally inactive. All samples contained DNA double labeled with the FRET donor and acceptor (Cy3 and Cy5). Significant changes were observed between 5S and the two promoter nucleosomes, including interesting differences when nucleosomes were diluted to sub-nM concentrations. They also measured the diffusion coefficient of the three samples and related it the compact packaging observed for the transcriptionally inactive sequence. The 5S sequence diffused 40% faster than the other two indicating that this sequence was tightly packed compared to transcriptionally active sequences.

Gansen et al. used multiparameter fluorescence detection (FRET efficiency, fluorescence lifetime and fluorescence anisotropy) along with FCS to reveal four different subspecies with different FRET efficiencies[22]. They assigned the subspecies as nucleosomes with high FRET efficiency (E ~ 0.5 corresponding to fully compact and completely assembled nucleosomes), medium FRET efficiency (E ~ 0.32 corresponding to slightly unwrapped nucleosomes with partial loss of histones), low FRET efficiency (E close to zero corresponding highly unwrapped species) and donor only nucleosomes (D-only). These intermediates were hypothesized as intermediates during nucleosome disassembly.

Koopmans et al. used FCS on selected photon bursts to identify subpopulations of nucleosomes in different conformations[23]. Use Alternate Excitation (ALEX), the authors were able to identify and distinguish photon bursts due to different nucleosome subpopulations: wrapped, unwrapped and disassembled. Their findings prove that the compact nucleosomes diffuse faster than naked DNA and that monovalent salt induces disassembly due to changes in ionic strength.

Poirier et al. used FCS to study conformational dynamics in nucleosome arrays[24]. They used a tri-nucleosome array where they used a DNA with three "601" positioning sequences and reconstituted them onto nucleosomes with the histone proteins. Use Mg^{2+}, the authors studied changes in diffusion coefficients due to compaction of the nucleosomes and also measured the rates for this compaction/decompaction of tri-nucleosomes.

Böhm et al. used FCS to study the intermediates during nucleosome disassembly induced by chanted in ionic strength[25]. Using fluorescent dyes on different histone proteins, the authors studied the change in diffusion coefficients upon addition of salt. The results suggested that the histone proteins are not lost in one step; in fact the histones H2A and H2B are released first, and upon further salt addition, the histone proteins H3 and H4 are released.

In this study, we measured the rates of DNA conformational change at sites which are further inside the nucleosome. Previously established equilibrium

constants indicate that the population of the unwrapped conformation decreases along the length of the DNA. Does this mean the rate of unwrapping decreases or rate of rewrapping increases or do both rates change along the length of the DNA?

We used Förster resonance energy transfer (FRET) coupled with Fluorescence correlation spectroscopy (FCS) to measure the rates of DNA re-wrapping at various sites from the end of the nucleosomal DNA to the middle. In collaboration with the Widom lab (who measured the DNA unwrapping rate using stopped-flow FRET measurements) we established the rates for spontaneous access to DNA sites. The results show that both the rewrapping and unwrapping rates decrease along the length of the nucleosomal DNA; however the unwrapping rate decreases by a greater magnitude. On the other hand, the decrease of re-wrapping rate is much less dramatic.

Materials and Methods

DNA and histones

Four Cy3-labeled DNA were prepared using PCR. Commercially synthesized Cy3-labeled DNA primer were used to incorporate Cy3 at positions 1, 35, 57 and 69 of the 147 bp "601" nucleosome positioning sequence[9]. Here on, these samples will be referred to as DA1, DA35, DA57 and DA69 respectively. In the case of DA1, a 5'Cy3 labeled primer was incorporated in the nucleosomal DNA using PCR. In the case of DA35 and DA57, the primers were purchased with amino-dT residue at the respective labeling positions and were subsequently

derivatized using amine-reactive Cy3 and purified using reverse-phase HPLC. For the Cy3 at position 69, four HPLC-purified long oligonucleotide primers, one containing a 5'-Cy3 end label at the position destined to become basepair 69 together with HPLC-purified unlabeled oligonucleotides of lengths 48 nt, 78 nt, and 99 nt. The four oligonucleotides were annealed, and the resulting 147 bp double stranded labeled DNA purified by preparative PAGE. All DNA sequence (except the sequence with Cy3 at position 69) contained a LexA consensus sequence (TACTGTATGAGCATACAGTA) into basepairs 8–27 to be used for stopped-flow FRET measurement. Recombinant *Xenopus* core histone proteins were expressed in *Escherichia coli*, purified in denatured form, refolded, reconstituted into histone octamers, and, when required, labeled with a sulfhydryl reactive Cy5 dye, as described. All systems prepared contained the engineered substitution H3 C110A, eliminating the unique wild type cysteine residue. Histones used with the DA1 and DA69 additionally contained the mutation H3 V35C. This engineered cysteine residue was derivatized with the sulfhydryl reactive Cy5 to create the FRET construct. Two additional engineered histone mutants were prepared and purified by the same methods: H2B T112C, used for DA35; and H4 L22C, used for DA57. The design of the systems ensured that in the wrapped conformation, the distance between the FRET pair is much shorter than the Förster distance resulting in a high FRET state (Fig. 2-3).

Nucleosome reconstitution

Cy3-labeled DNAs were reconstituted with Cy5-labeled histone octamers in the presence of excess salmon sperm DNA as a histone buffer, using salt gradient double dialysis. The resulting nucleosomes were purified away from any free 601 DNA, the competitor DNA, any non-nucleosomal aggregates, and any remaining free dye, by sucrose gradient ultracentrifugation as described. Nucleosome concentrations were determined from the Cy3 absorbance. All samples were prepared in the Widom lab at Northwestern University.

Fluorescence correlation spectroscopy

FCS measurements were carried out in two independent confocal systems. The first system (Fig. 2-4 and Fig. 2-5) was a home-built confocal setup. A 532 nm CW laser from Crystalaser (Reno, NV) was expanded and collimated to a Gaussian beam profile using a pair of lenses. The lenses were chosen such that the expanded laser beam just filled the back aperture of the objective (Olympus Plan Apo 100X 1.4NA). Positioning the second lens on a two-axis stage (Newport 460A series) permitted fine tuning of the size of the beam and its collimation The laser power was attenuated to the desired power using neutral density filters. A pair of two-axis mirrors was used to steer the beam and the laser is then directed onto a 45^0 dichroic mirror (Omega Opticals XF2017). The dichroic mirror was used to reflect the laser while transmitting the emitted fluorescence. The reflected beam entered the back aperture of the Olympus objective and focused to a

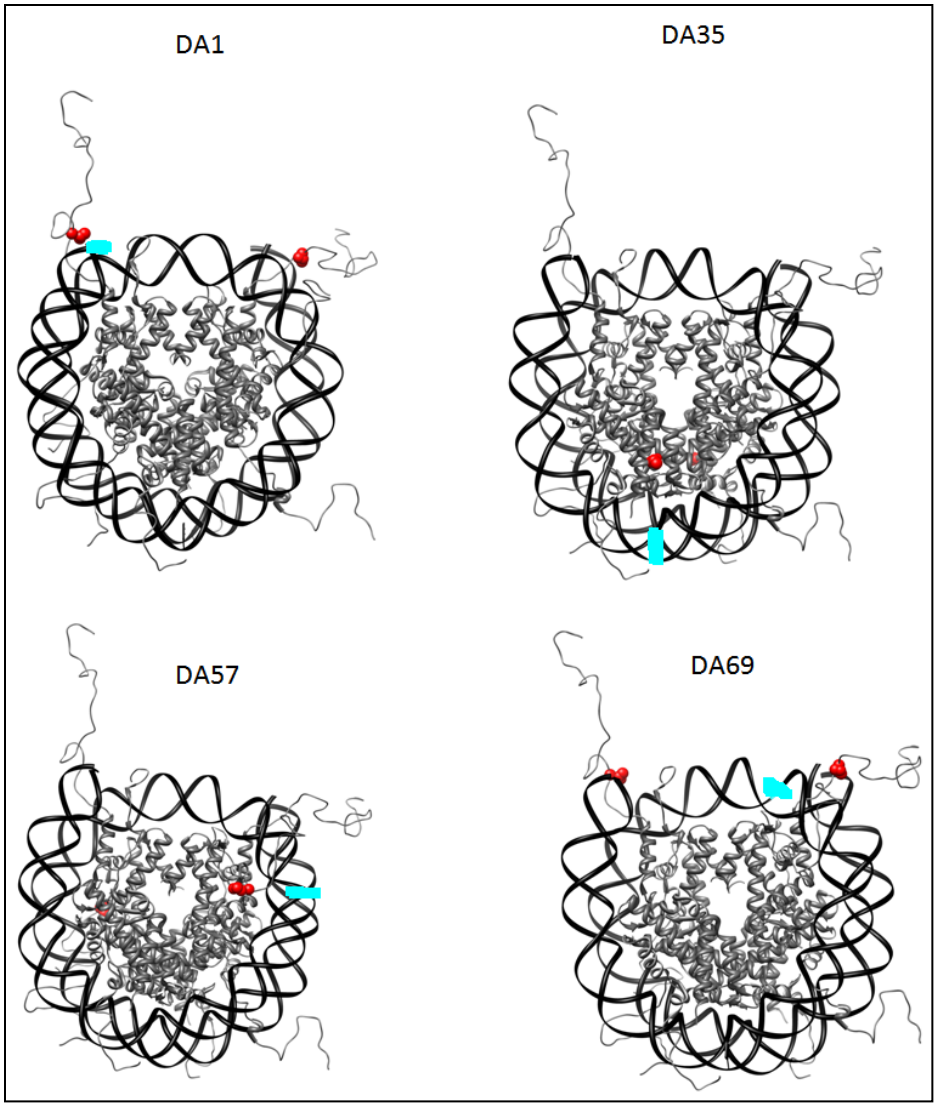

Fig. 2-3: FRET constructs to study position dependent nucleosome site-exposure kinetics. The FRET donor Cy3 (cyan) is moved along the length of the DNA from the 5' end of the "601" DNA (DA1) to the 35th, 57th and 69th base (DA35, DA57 and DA69 respectively. The FRET acceptor (Cy5) is attached to engineered cysteine residues (H3 V35C for DA1 and DA69, H2B T112C for DA35 and H4 L22C for DA57).

diffraction limited spot in the sample. The sample was mounted on a dry clean glass coverslip (Fisher Scientific #1.5) within a perfusion chamber (Grace Biolabs PC8R-0.5). The objective assembly was housed on an optical stage (Thorlabs) and the objective position is adjusted using a micrometer of 750 nm resolution. A two-axis piezo scanning stage (P-541.2Sl Physik Instrumente) was used to scan the stage when necessary. The piezo actuator worked in both open- and closed-loop formats with the closed-loop version having feedback from high resolution strain gauge sensors. The nanopositioner was controlled using analog outputs from a DAQ board (PCI 6733 National Instruments). Fluorescence emission from the sample was collected by the same objective lens and passed through the primary dichroic mirror. The fluorescence emission was then passed through a lens of known focal length and focused onto a pinhole (50 μm) which is positioned at the conjugate image plane of the focusing lens. The whole pinhole assembly was mounted on a cage system (Thorlabs) and supported by heavy posts to minimize the drift and to maintain collinearity. The light coming out of the pinhole was then collimated again using a second lens and then was split into two beam paths using a second dichroic mirror (Omega Opticals XF2021). The two beam paths belong to the FRET donor (Cy3) and FRET acceptor (Cy5) respectively. The light beams were then steered using a pair of two-axis mirrors and focused on the sensitive area of a single-photon counting module, (SPCM-AQR-14, Perkin Elmer). Additional optical filters (Omega optical 3rd generation

filters 3RD560-620 and 3RD670-740 for Cy3 and Cy5) were used to minimize background in either channel.

The second confocal system was constructed using a Nikon Eclipse TE2000-U microscope (Nikon, Melville, NY). A 532nm CW Nd:YVO4 laser (Millenia Xs, Coherent, Santa Clara, CA) was used as the excitation source and focused onto the sample using a 100X 1.4NA oil immersion objective (Plan Apo, Nikon, Melville, NY). The same objective was used to collect the emitted photons. The donor and acceptor signals were separated using a dichroic mirror (Q660LP Chroma Technology Corp., Rockingham, VT) and detected using two silicon avalanche photodiodes (SPCM-AQR-12, Perkin-Elmer, Fremont, CA). Appropriate filters were used in front of the detectors to further reduce background and crosstalk (BP570/40 for Cy3 and BP670/40 for Cy5, Chroma Technology, Rockingham, VT). This system was used to increase the confocal volume so as to increase the diffusion time of the molecules. To do this, no pinhole was used in the detection path and the observation volume is limited the active area of the detectors (~200 μm diameter).

The detector output was collected either by PC counter boards (PCI-6602 National Instruments) for further data analysis Matlab, or by a multi-tau digital hardware correlator (ALV-5000, ALV Gmbh) for direct acquisition of auto- and cross-correlation traces.

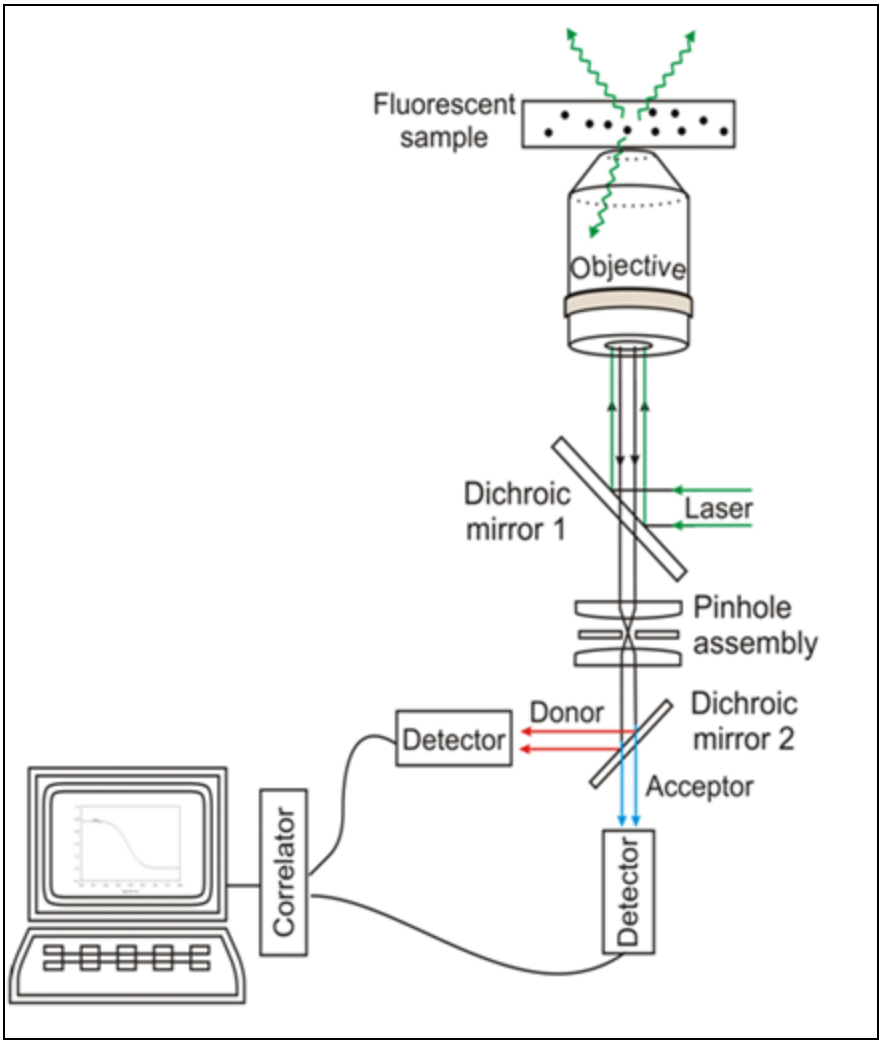

Fig. 2-4: Schematic of the FCS setup. A 532nm laser was focused onto the sample using a 100X 1.4 NA oil immersion objective. Fluorescence from the sample was collected using the same objective and spatially filtered using a pinhole. The signal was split into the donor and acceptor signals using a dichroic mirror and focused onto two independent detectors. The outputs of the detectors were collected using a correlator and analyzed in the computer.

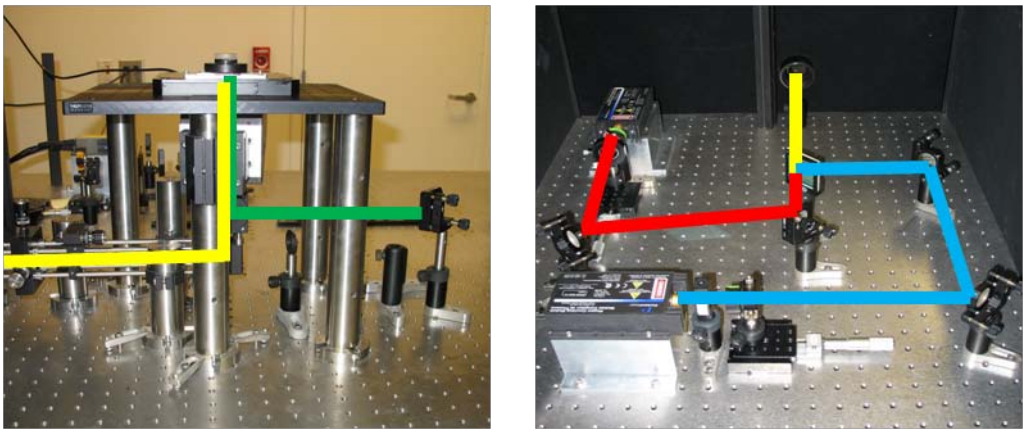

Fig. 2-5: Photograph of FCS setup. Left: The excitation part of the setup consisting of the laser (green) and the emitted fluorescence (yellow). Right: The detection part of the setup. The emitted fluorescence is split into the donor (blue) and acceptor (red) signals using a dichroic mirror. The colors of the lines are artificial and are added to aid in visual representation only.

All experiments were performed with 10 nM donor-acceptor nucleosome samples in 1 X TE buffer in the presence of 100 nM unlabeled nucleosome core particles to decrease the likelihood of nucleosome dissociation. Background contributions were measured under the same conditions in the absence of labeled nucleosomes, and were less than 0.5% (donor detector) and 1.5% (acceptor detector) of the measured signals in the presence of fluorescent nucleosomes. Crosstalk (donor signal measured in the acceptor channel) was estimated as 5% using a donor-only DNA sample. The contributions of the acceptor signal in the donor channel were negligible. Fluctuations in fluorescence intensities of both the donor and acceptor are due to translational diffusion as nucleosomes diffuse through the observation volume, and due to DNA kinetic transitions that affect the distance between the donor and acceptor probes. In the previous work[8], the ratio of the donor autorocorrelation decays of the donor-only and donor-acceptor labeled samples was used to isolate the contributions of these conformational transitions from those due to translational diffusion. This approach requires that the two experiments are carried out under identical conditions so that the diffusion contributions are properly cancelled. However, some experimental variables, including sample concentration, size and shape of the observation volume, inhomogeneities in cover slip thickness, etc, are hard to control precisely between measurements. Use of two samples to obtain correlation functions is impractical to replicate in cells, membranes and other substrates. Subsequent work

demonstrated that these experimental difficulties can be overcome by analyzing the ratio of the donor autocorrelation and the donor-acceptor cross-correlation functions (G_{DD}/G_{DA}) measured for the doubly-labeled sample[17]. The auto- and cross-correlations were calculated from the same stream of photons, so they were acquired simultaneously in a single experiment, eliminating all sources of experimental artifacts that are associated with the need of conducting two experiments in equal conditions.

The analytical expression for the correlation functions G_{DD} and G_{DA} contain contribution from both diffusion and kinetic transitions. However the ratio of the two correlation function is independent of contributions from diffusion and yields a function that can fitted with the timescale of conformational dynamics. Although the ratio G_{DD}/G_{DA} is independent of the diffusion contributions, its signal-to-noise ratio depends strongly on the relative timescales of diffusion and conformational dynamics. In the cases of nucleosomes, the timescales of conformational dynamics were much slower than the diffusion timescales. Hence preliminary experiments with the samples DA57 and DA69 yielded poor signal to noise in the ratio G_{DD}/G_{DA}. This is because in the first optical setup, with the use of a pinhole, the observation volume was restricted and the corresponding diffusion timescale for the nucleosomes were a few milliseconds. To overcome this limitation, we performed experiments with the DA57 and DA69 samples in the second optical setup with no pinhole. The removal of the pinhole increases the

observation volume and as a result, the diffusion timescales is higher. However since the size of the observation volume has no bearing on the timescales of conformational dynamics, we were able to recover the timescales for these samples. In FCS, the amplitude of fluctuations is inversely proportional to the mean number of molecules in the observation volume. As a result of removing the pinhole and increasing the observation volume, the mean number of molecules in the observation volume increased and hence the amplitude decreased. This demanded the total acquisition time for this optical setup to be higher to achieve acceptable signal-to-noise.

The analytical expressions for the auto- and cross-correlation functions of a two-state system in equilibrium were derived in previous work[17], and can be written as:

$$G_{xy}(\tau) = T(\tau)[1 + C_{xy} \exp\left(-\frac{\tau}{\tau_R}\right)] \quad \text{2-1}$$

where $T(\tau)$ represents the contribution of translational diffusion, $\tau_r = (k_{12} + k_{21})^{-1}$ represents the relaxation time of the reaction, k_{12} and k_{21} represent the unwrapping and rewrapping kinetic rate constants, and C_{xy} is a coefficient that depends on the equilibrium constant of the reaction ($K = k_{12} / k_{21}$) and the FRET efficiencies (E) in each state:

$$C_{DD} = \frac{K(E_1 - E_2)^2}{(1 - E_1 + K(1 - E_2))^2} \quad \text{2-2}$$

$$C_{DA} = \frac{K(E_1 - E_2)^2}{(1 - E_1 + K(1 - E_2))(E_1 + KE_2)} \qquad 2-3$$

The ratio G_{DD}/G_{DA} can be thus written as

$$\frac{G_{DD}}{G_{DA}}(\tau) = \frac{1 + C_{DD}\exp\left(-\frac{\tau}{\tau_R}\right)}{1 + C_{DA}\exp\left(-\frac{\tau}{\tau_R}\right)} \qquad 2-4$$

An important feature of this expression is that although the amplitude of the G_{DD}/G_{DA} decay depends on variables that we do not know, the characteristic time of the decay is directly the relaxation time of the reaction ($\tau_r = (k_{12} + k_{21})^{-1}$). Because nucleosomes spend most of the time in the closed conformation ($k_{12} << k_{21}$), the relaxation time is dominated by the closing transition (i.e. ($\tau_R = k_{21}^{-1}$)). Consequently, our method of analysis yields the rate of the wrapping reaction (k_{21}) with much higher confidence than the equilibrium constant or the rate of the unwrapping reaction. The amplitude of the decay depends on other experimental factors such as crosstalk (i.e. donor photons that leak into the acceptor detector) and the presence of donor-only species (such as free DNA, or nucleosomes that lack the acceptor molecule). In contrast, the relaxation time is not affected by any of these experimental concerns.

Eq. 4 can be manipulated to yield the relaxation time independently of the amplitude as follows:

$$\frac{\frac{G_{DD}}{G_{DA}}(0)-1}{\frac{G_{DD}}{G_{DA}}(\tau)-1}=\frac{1}{1+C_{DA}}\exp\left(\frac{\tau}{\tau_R}\right)+\frac{C_{DA}}{1+C_{DA}} \qquad 2.5$$

$$\ln\left[\frac{\frac{G_{DD}}{G_{DA}}(0)-1}{\frac{G_{DD}}{G_{DA}}(\tau)-1}\right]\approx\ln\left[\frac{1}{1+C_{DA}}\right]+\frac{\tau}{\tau_R}\qquad for\ \exp\left(\frac{\tau}{\tau_R}\right)\gg C_{DA} \qquad 2.6$$

Therefore, a logarithmic plot of Eq.5 is linear at long times with a slope that equals the reciprocal of the relaxation time independently of the experimental variables included in the coefficients C_{xy}.

Results

Fluorescence Correlation Spectroscopy was performed on all four nucleosome samples: DA1, DA35, DA57 and DA69. The nucleosomes are specifically labeled with a FRET donor dye (Cy3) placed at bases 1, 35, 57 and 69 from one end. The FRET acceptor dye (Cy5) was attached to engineered cysteine residues (H3 V35C C110A for DA1 and DA69, H2B T112C for DA35; and H4 L22C for DA57). This resulted in a donor-acceptor distance of ~2nm in all cases when the nucleosomes were in the wrapped conformation. This distance is less than the Förster distance for this dye pair (~5.5nm) and hence the FRET efficiency is very high in this state. Since the nucleosomes consists of two copies of each histone, a second acceptor molecules is present but is much further away

from the donor molecule and its contribution to FRET signal is low. As the nucleosomes unwrap, the distance between the FRET donor and acceptor molecules increase resulting in the decrease of the FRET efficiency. This conformational change results in fluctuations of the fluorescence signal of both the donor and acceptor and contributes to the auto- and cross-correlation curves. As mentioned in the methods, since the equilibrium constant is shifted to the wrapped state, the rewrapping rate (k_{21}) is much faster than the unwrapping rate (k_{12}). The time constant for this kinetic process, τ_R, is thus dominated by the rewrapping rate and FCS analysis yields accurate measurement of the rewrapping rate. The Widom lab used stopped-flow FRET measurements to measure the position dependent unwrapping rate. To do this, a LexA binding sequence was positioned at various distances from the end and the accessibility by LexA was measured. As the LexA protein binds to the target site, the FRET efficiency decreases and unwrapping rates can be recovered.

Donor autocorrelation (G_{DD}) and donor-acceptor crosscorrelation (G_{DA}) functions were calculated from the same photon streams. This removes the need of using a donor-only labeled sample as a control that was used in the earlier work hence reducing some experimental error. The rates obtained for DA1 sample is in good agreement with results obtained in the earlier work.

As the donor was moved further into the DNA, the rewrapping rate k_{21} decreased from 21 s^{-1} to 15 s^{-1} for the DA35 sample and decreased further to 1.8

s^{-1} and 1.4 s^{-1} for the DA57 and DA69 samples. These corresponded to an unwrapped conformation lifetime of ~48 milliseconds for DA1 and ~65 milliseconds for DA35, ~560 milliseconds for DA57 and ~740 milliseconds for DA69 samples.

The Widom lab performed stopped-flow FRET experiments using LexA binding to target sequences. The results of these experiments revealed that the unwrapping rate (k_{12}) was ~4 s^{-1} for sites the end of the nucleosomal DNA. This value remained the same when the LexA binding sequence was moved 8 basepair into the DNA. However further displacement of the LexA binding sequence to the 18^{th} basepair resulted in a ~250 fold decrease of the unwrapping rate to ~0.016 s^{-1} and when the LexA binding sequence was moved to the 28^{th} basepair, the unwrapping rate decreased to ~0.0017 s^{-1}. The rewrapping rates measured by FRET-FCS analysis are summarized in table 2-1 and presented along with the unwrapping rates in Fig. 2-7.

Table 2-1: Re-wrapping rates measured by FRET-FCS

DNA construct	k_{21}	$\tau_{unwrapped} = k_{21}^{-1}$
DA1	21 s^{-1}	48 ms
DA35	15 s^{-1}	65 ms
DA57	1.8 s^{-1}	560 ms
DA6957	1.4 s^{-1}	740 ms

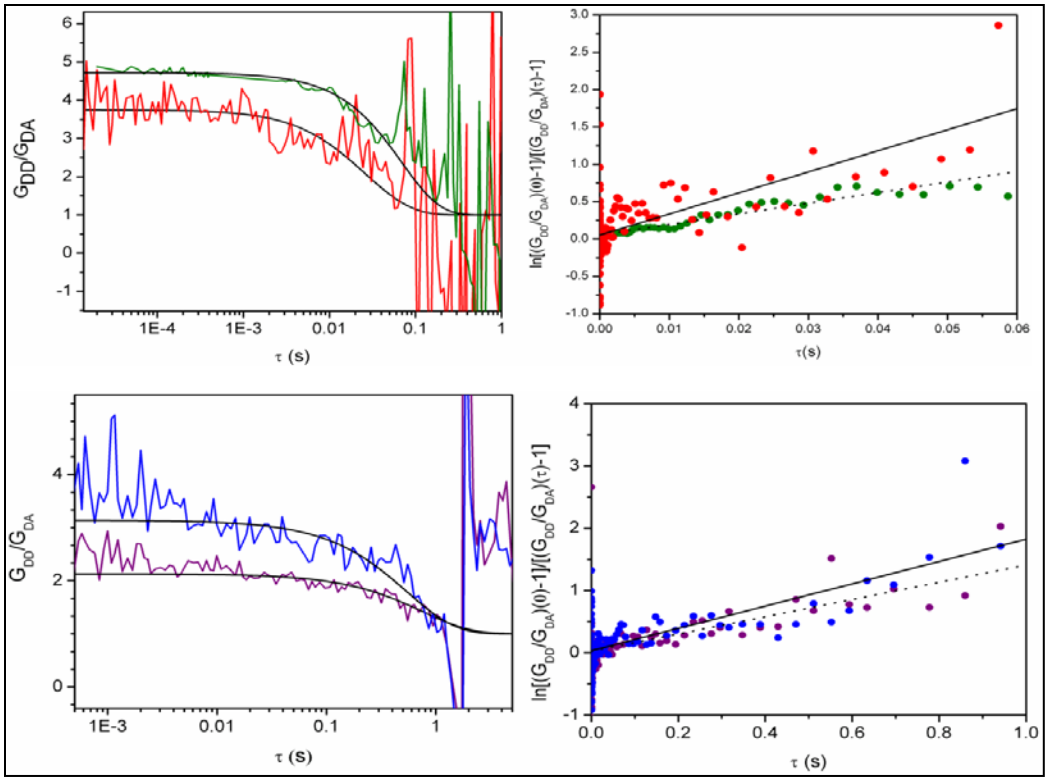

Fig. 2-6: Position-dependent rewrapping rates measured by FRET-FCS. Left: Ratios of donor autocorrelations (G_{DD}) to donor-acceptor cross correlations (G_{DA}) vs. lag time τ. Results for DA1 in red, DA35 in green, DA57 in blue and DA69 in violet. Black lines are fit according to Eq. 2.4. Right: Ratios plotted in a logarithmic fashion according to Eq. 2-6. Black lines represent linear fits, whose slope equals the reciprocal of the relaxation time at long lag times.

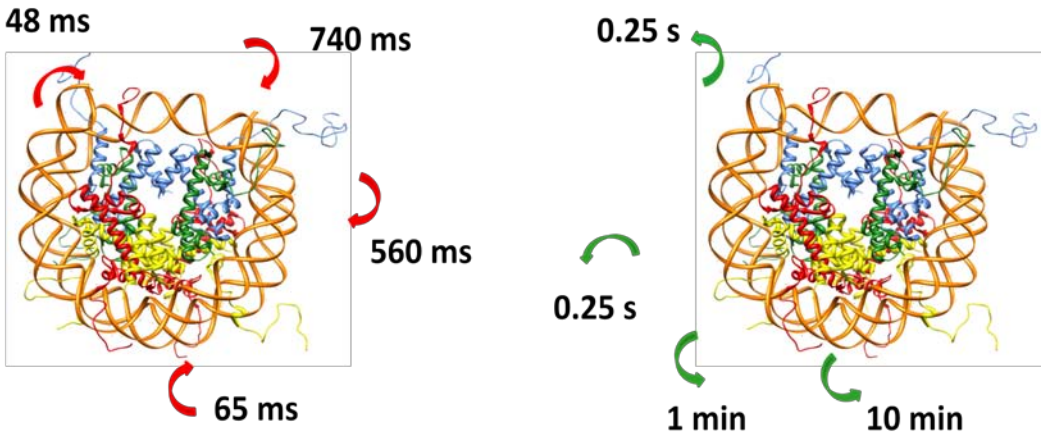

Fig. 2-7: Summarized lifetimes of open and closed conformations. Left: Position dependent lifetime of open conformations measured using FRET-FCS analysis. Red arrows mark the base position where the FRET donor (Cy3) was attached. Right: Position dependent lifetime of closed conformations using stopped-flow FRET analysis. Green arrows mark the position at which the LexA binding sequence was placed.

Discussion

Position dependent site exposure kinetics was measured using independent methods. FRET-FCS analysis was used to unravel the rewrapping rates (k_{21}) of DNA onto the nucleosomes starting from the nucleosome end progressively to the middle of the DNA while stopped flow FRET experiments were performed to measure the unwrapping rates (k_{12}). The results indicate that while the unwrapping rate decreases dramatically for DNA sites along the length of the DNA, the rewrapping rate decreases albeit gradually. The equilibrium constants for the unwrapping-rewrapping event led to the hypothesis that either the unwrapping rate decreases along the length of the DNA or the rewrapping rate increases. However contrary to the hypothesis; both the unwrapping and the rewrapping rates decreased for target sites further along the DNA. The gradual decrease in the rewrapping rate compensates for the dramatic decrease in the unwrapping rate to maintain the equilibrium constant.

These results indicate that the nucleosomal DNA unwraps progressively in steps. Since the unwrapping rate decreases in a dramatic fashion, greater energy is required to unwrap longer lengths of DNA. This could also suggest that while shorter lengths of DNA are exposed, opportunistic enzymes could bind to the exposed target sites and prevent this stretch of DNA from rewrapping. This could facilitate a further unwrapping event for a second enzyme to bind to its target site. Such co-operative binding events are often found in various cellular processes.

To summarize the results, equilibrium constants measurements show that the wrapped conformation predicted by X-ray crystallography is not a static state; in fact the DNA unwraps from the nucleosomes and becomes accessible to regulatory proteins. Target site accessibility depends on the position of the site with the nucleosome. Sequences near the end of the DNA are accessible with greater ease than for sites near the middle. This unwrapped state, however, is not long lived and rapidly falls back into the wrapped conformation.

References

(1) Richmond, T. J.; Davey, C. A. *Nature* **2003**, *423*, 145-50.

(2) Teif, V. B.; Rippe, K. *Nucleic Acids Res* **2009**, *37*, 5641-55.

(3) Whitehouse, I.; Rando, O. J.; Delrow, J.; Tsukiyama, T. *Nature* **2007**, *450*, 1031-5.

(4) Ng, H. H.; Ciccone, D. N.; Morshead, K. B.; Oettinger, M. A.; Struhl, K. *Proc Natl Acad Sci U S A* **2003**, *100*, 1820-5.

(5) Polach, K. J.; Widom, J. *J Mol Biol* **1995**, *254*, 130-49.

(6) Anderson, J. D.; Thastrom, A.; Widom, J. *Mol Cell Biol* **2002**, *22*, 7147-57.

(7) Li, G.; Widom, J. *Nat Struct Mol Biol* **2004**, *11*, 763-9.

(8) Li, G.; Levitus, M.; Bustamante, C.; Widom, J. *Nature structural & molecular biology* **2005**, *12*, 46-53.

(9) Anderson, J. D.; Widom, J. *J Mol Biol* **2000**, *296*, 979-87.

(10) Hodges, C.; Bintu, L.; Lubkowska, L.; Kashlev, M.; Bustamante, C. *Science* **2009**, *325*, 626-8.

(11) Mavrich, T. N.; Ioshikhes, I. P.; Venters, B. J.; Jiang, C.; Tomsho, L. P.; Qi, J.; Schuster, S. C.; Albert, I.; Pugh, B. F. *Genome Res* **2008**, *18*, 1073-83.

(12) Luse, D. S.; Spangler, L. C.; Ujvari, A. *J Biol Chem*, *286*, 6040-8.

(13) Neuweiler, H.; Doose, S.; Sauer, M. *Proc Natl Acad Sci U S A* **2005**, *102*, 16650-5.

(14) Kim, J.; Doose, S.; Neuweiler, H.; Sauer, M. *Nucleic Acids Res* **2006**, *34*, 2516-27.

(15) Bonnet, G.; Krichevsky, O.; Libchaber, A. *Proc Natl Acad Sci U S A* **1998**, *95*, 8602-6.

(16) Kelbauskas, L.; Chan, N.; Bash, R.; Yodh, J.; Woodbury, N.; Lohr, D. *Biochemistry* **2007**, *46*, 2239-48.

(17) Torres, T.; Levitus, M. *J Phys Chem B* **2007**, *111*, 7392-400.

(18) Altan-Bonnet, G.; Libchaber, A.; Krichevsky, O. *Phys Rev Lett* **2003**, *90*, 138101.

(19) Petrov, E. P.; Ohrt, T.; Winkler, R. G.; Schwille, P. *Phys Rev Lett* **2006**, *97*, 258101.

(20) Kelly, S. M.; Pabit, S. A.; Kitchen, C. M.; Guo, P.; Marfatia, K. A.; Murphy, T. J.; Corbett, A. H.; Berland, K. M. *Proc Natl Acad Sci U S A* **2007**, *104*, 12306-11.

(21) Kelbauskas, L.; Chan, N.; Bash, R.; DeBartolo, P.; Sun, J.; Woodbury, N.; Lohr, D. *Biophys J* **2008**, *94*, 147-58.

(22) Gansen, A.; Valeri, A.; Hauger, F.; Felekyan, S.; Kalinin, S.; Toth, K.; Langowski, J.; Seidel, C. A. *Proc Natl Acad Sci U S A* **2009**, *106*, 15308-13.

(23) Koopmans, W. J.; Buning, R.; Schmidt, T.; van Noort, J. *Biophys J* **2009**, *97*, 195-204.

(24) Poirier, M. G.; Oh, E.; Tims, H. S.; Widom, J. *Nat Struct Mol Biol* **2009**, *16*, 938-44.

(25) Bohm, V.; Hieb, A. R.; Andrews, A. J.; Gansen, A.; Rocker, A.; Toth, K.; Luger, K.; Langowski, J. *Nucleic Acids Res*.

Chapter 3

PROXIMITY FACTOR CORRELATION: APPLICATIONS TO CONFORMATIONAL DYNAMICS AND LIMITATIONS

Introduction

Fluorescence Correlation Spectroscopy (FCS) has been applied to study and measure the kinetic parameters of various conformational dynamics of biomolecules and chemical reactions. By conveniently labeling the molecules with fluorophore(s), these processes can lead to fluctuations in the fluorescence signal, and their kinetic information can be recovered by fitting the FCS decay curves to appropriate models. The processes include photophysical reactions like triplet state dynamics[1] or photoconversion[2], chemical reactions[3] and conformational dynamics[4-6]. Most of the studies were done on molecules diffusing in solution or *in vivo* which leads to an open observation volume. Hence the resulting fluorescence correlation curves contain contributions from both conformational dynamics and translational diffusion (discussed in Chapter 2). One way to isolate the contributions from conformational dynamics is to remove translation diffusion by immobilizing the molecules of interest to the surface thereby eliminating diffusion. This has been successfully employed to study conformation dynamics of RNA three-helix junctions[7], coiled-coil peptides[8] and DNA hairpins complexed with the HIV-1 NC protein[9]. However, surface immobilization is not applicable in many cases due to the fact that although most

nucleic acid substrates are robust enough, proteins, in most cases, interact with the surface and their activity is lost. Also, in cases where surface immobilization is employed, the temporal resolution is determined by the camera, that is often employed under such conditions, and is typically lower than the detectors used in routine FCS experiments performed on diffusing molecules. Hence, in the effort to keep the biomolecules in their active state, the studies are performed on freely diffusing molecules in their native state. Under these conditions, FCS decay curves contain both kinetic and diffusion components and a more detailed analysis of the correlation decay curves need to be done to isolate the contributions from conformational dynamics.

In situations where kinetic transitions results in fluctuations of the fluorescence signal, the autocorrelation function contains contributions from kinetic transitions as well as diffusion. The autocorrelation curve for such a system is given by

$$G(\tau) = T(\tau) \cdot X(\tau) \qquad 3\text{-}1$$

where $T(\tau)$ and $X(\tau)$ are the contributions from diffusion and kinetic transitions respectively. To express the autocorrelation function as a product of the two contributions, the diffusion coefficient of the biomolecule in different conformations is assumed to be the same.

For a two-state kinetic transition model, $X(\tau)$ can be described by an exponential decay given by

$$X(\tau) = 1 + \exp\left(-\frac{\tau}{\tau_R}\right) \qquad 3\text{-}2$$

where τ_R is the characteristic relaxation time of the kinetic process.

There are three scenarios that arise here: scenario one where the characteristic time of the chemical reaction (τ_R) is much lower (faster) than the characteristic diffusion time (τ_D), scenario two where the reaction time is slower than the diffusion time and finally a scenario where the two timescales are similar. In the first case ($\tau_R << \tau_D$), molecules enter the observation volume and undergo multiple transitions between the states of high and low quantum yield before exiting the volume. This will lead to a temporal separation in the contributions from kinetics and contribution of diffusion to the correlation decay curve. However, for the other cases ($\tau_D << \tau_R$ and $\tau_D \sim \tau_R$), there is an overlap of these two time scales and the separation between the two contributions is minimal. Using Eq. 3-2 and Eq. 1-3, theoretical predictions of correlation functions can be made. Fig. 3-1 shows the correlation functions as predicted by these equations. As it can be seen, for the case where $\tau_R << \tau_D$, there is clear separation between the contributions from conformational dynamics and diffusion. However, for other cases, the separation is not trivial and one needs to isolate the contributions to extract kinetic timescales.

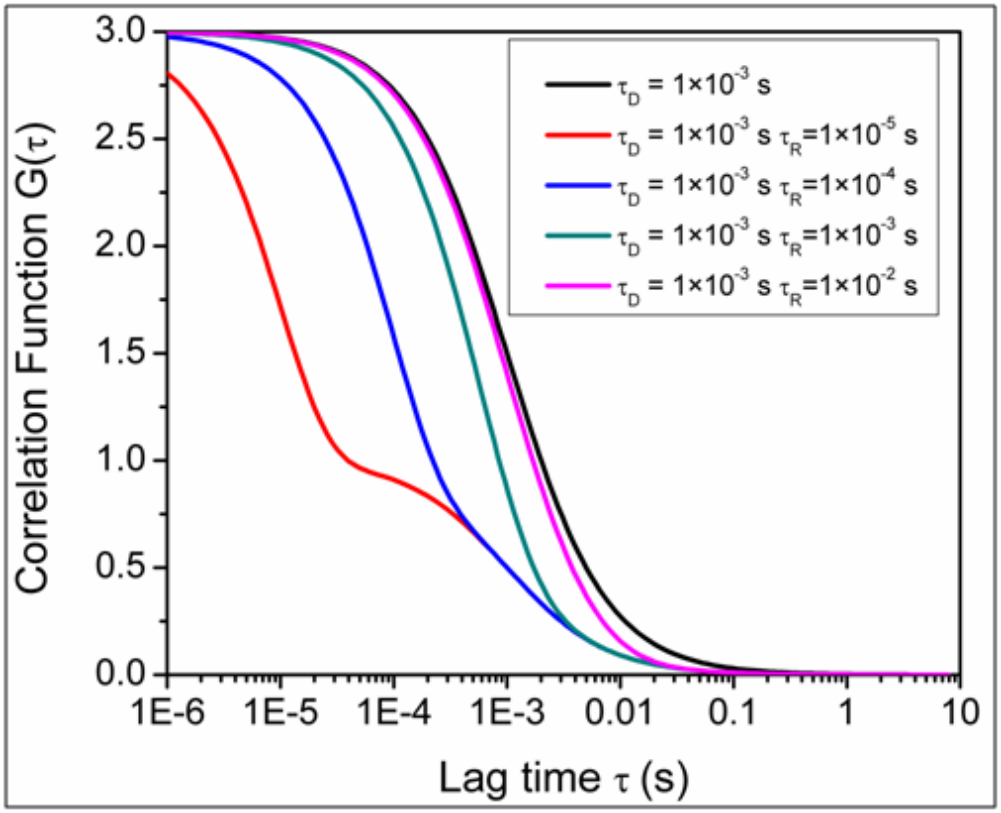

Fig. 3-1: Theoretical predictions of correlation functions. Correlation functions were calculated according to Eq. 3-1 for cases with different relaxation times. For cases where the kinetic transitions were much faster than diffusion times ($\tau_R << \tau_D$), the contributions from kinetic transitions and diffusion to correlation functions are visually separated. However for other cases ($\tau_R << \tau_D$ and $\tau_R \sim \tau_D$), there is an overlap between the contributions.

To overcome the limitations that arise from the overlap of the contributions from kinetics and diffusion, many indirect and alternative approaches have been developed. Bonnet et al.[10] used a fluorophore-quencher double labeled DNA hairpin sample to measure the fluorescence correlation decay curve and compared it to the correlation decay curve of fluorophore-only control sample. DNA can adopt a hairpin conformation and can undergo transition between a closed and open conformation as shown in Fig. 3-2. While the correlation decay curve for the dual labeled sample contained contributions from both kinetics and diffusion, the one for the control sample contained contributions from diffusion only. By taking a ratio of the two, the kinetic contributions can be isolated and fit to appropriate kinetic models. Fig. 3-3 shows the correlation curves obtained with both samples and the ratio of the two correlation curves fitted to an exponential function.

Similar approaches have been used to measure the kinetics of conformational dynamics of mononucleosomes[4,9,11], conformational dynamics of nucleosome arrays[12] and DNA interactions with HIV-1 nucleocapsid protein[13].

The goal of this thesis is to measure the timescales for the conformational dynamics of nucleosomes. An earlier study revealed that the relaxation time for the unwrapping and rewrapping of DNA near the exit of a nucleosome complex is 50 ms[4] which is slower than the diffusion time of the nucleosomes (~1 ms for usual confocal setups). Since the correlation decay is dominated by diffusion, the

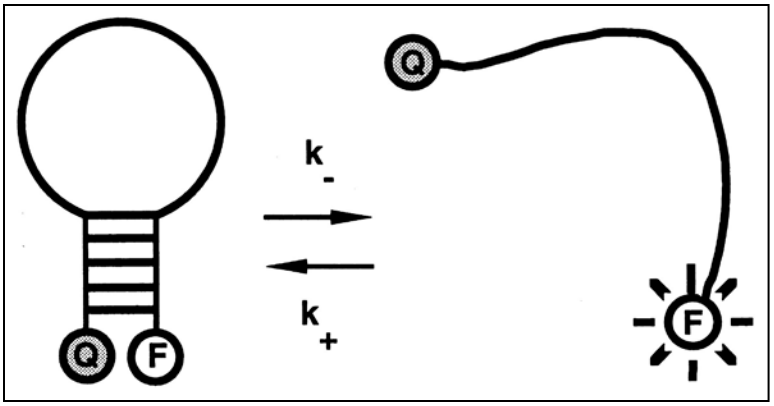

Fig. 3-2: Cartoon representation of conformational dynamics of DNA hairpins studied by Bonnet *et al.* [10] Briefly, a fluorophore (F) and a quencher (Q) are covalently attached to ends of DNA that forms a hairpin loop. As the DNA hairpin undergoes conformational dynamics between closed (left) and open (right) states, the fluorescence signal fluctuates between quenched and unquenched levels. The conformational dynamic rates were recovered using FCS. Reprinted with permission. This cartoon can be used to represent any kinetic transition undergoing two-state mechanism.

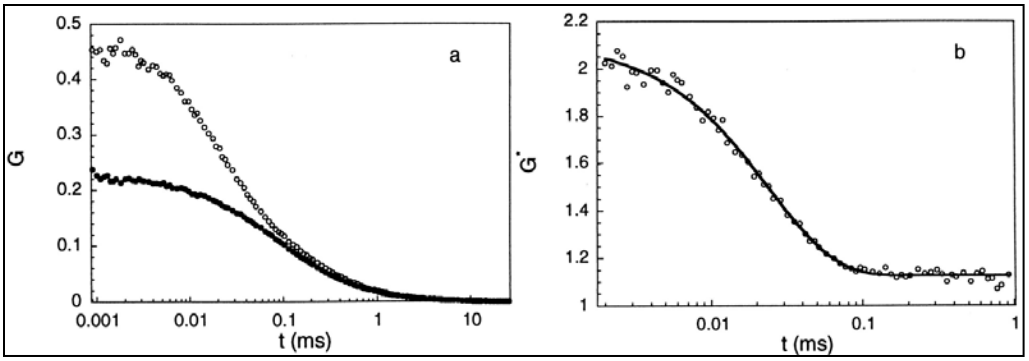

Fig. 3-3: Results of FCS experiments from Bonnet *et al.*[10]. Autocorrelation curves were measure for DNA hairpins with quencher (○) and without (•). FCS curves for DNA hairpins with quencher contain contributions from both kinetic transitions and diffusion while FCS curves for control samples (without quencher) only contain contributions from diffusion. As seen in Eq. 3-1, the ratio of the two curves separates the kinetic contributions. Reprinted with permission.

contributions from kinetic transitions are buried in the tail of the correlation functions. The use of the methodology developed by Bonnet et al.[10] for nucleosomes results in functions that have high noise. To measure nucleosome dynamics, we were in search of alternative methods which would isolate the contributions from kinetic transitions from the contributions from diffusion.

Another alternative was suggested by Klenerman and co-workers[14,15] to separate the contributions from kinetic transitions and diffusion. This method involves using a FRET pair (a donor *D* and an acceptor *A*) to label the molecule of interest and then correlating the fluctuations of a parameter called proximity factor *p*. The proximity factor is defined as

$$p = \frac{I_A}{I_A + I_D} \qquad 3\text{-}3$$

where I_{A} and I_{D} are the acceptor and donor intensities measured in the respective detectors. This factor intuitively depends only on the state of the molecule (high FRET or low FRET state) but not on the position of the molecule within the confocal volume. Although I_{A} and I_{D} depend on the position of the molecule within the confocal volume, the proximity factor should only depend on the FRET efficiencies of the states and thus, in principle, the correlation function of the proximity factor should have contributions only from kinetics and not from diffusion. The correlation function of proximity factor is defined as

$$G_p(\tau) = \frac{\langle \delta p(t)\, \delta p(t+\tau) \rangle}{\langle p(t) \rangle^2} \qquad 3\text{-}4$$

The authors then fitted the correlation of the proximity factor ($G_p(\tau)$) to a stretched-exponential function as shown in Fig. 3-4

$$G_p(\tau) = G_p(0)\exp\left(-\left(\frac{\tau}{\tau_R}\right)^{\beta}\right) \quad 3\text{-}5$$

where τ_R is the relaxation time of the kinetic process, $G_P(0)$ is the amplitude of the correlation function at lag time $\tau = 0$ and β is a stretch parameter used to interpret the mechanism of kinetic transitions. A value of β close to one reflects a simple two-state mechanism while a value of β less than one indicates multi-step kinetic transitions.

In this study, we explore the applicability of this method to study nucleosome dynamics. We used Monte Carlo simulations as well as experiments with nucleosomes to demonstrate that this method is applicable to cases where $\tau_R << \tau_D$ only. For other cases, especially for nucleosomes where $\tau_R > \tau_D$, this method fails. When we initially applied this methodology to nucleosomes, we obtained timescales much faster than reported before. This motivated us to look further into the method and understand the concept.

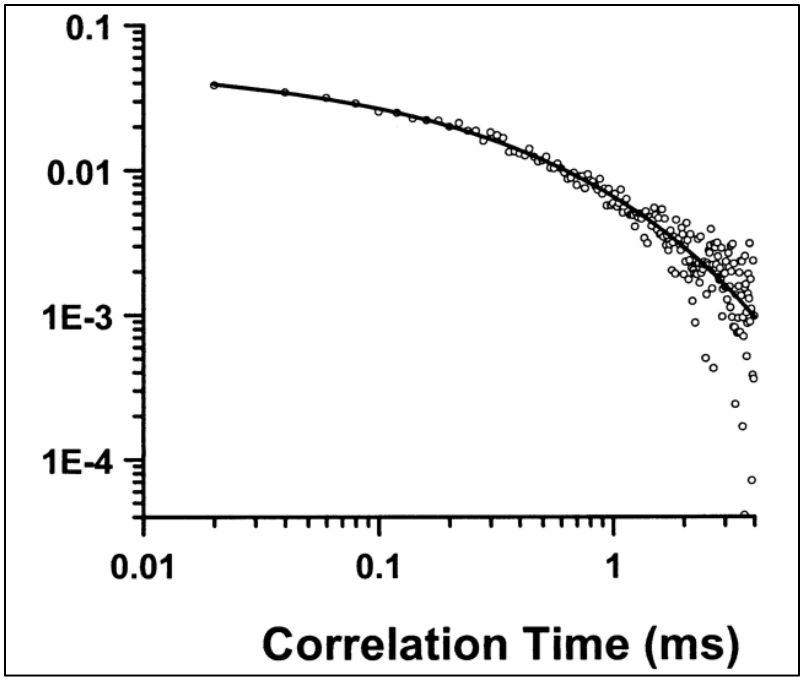

Fig. 3-4: Correlation function of proximity factor ($G_p(\tau)$) measured by Klenerman and co-workers[14] for DNA hairpins labeled with TMR and Cy5 as FRET donor and acceptor. Reprinted with permission.

Materials and Methods

Fluorescence experiments: FCS and proximity factor correlation experiments were carried out in a home-built confocal system consisting of a 532 nm CW laser (Crystalaser, Reno, NV) which was expanded and collimated to fill the back aperture of a 100X 1.4 NA Olympus PlanApo oil immersion objective. The emitted fluorescence was then collected using the same objective and was passed through a 50 μm pinhole assembly which rejected out-of-focus light and created confocal observation volume. The donor and acceptor fluorescence was separated using a dichroic mirror (Omega XF2021) and were detected using single photon counting modules (SPCM-AQR14, Perkin Elmer Optoelectronics). For FCS experiments, the output of the detectors were correlated using a multi-tau hardware digital correlator (ALV-5000, ALV Gmbh, Germany) while for the generalized polarization experiments, the signals were collected using a DAQ board (PCI-6602, National Instruments, Austin) with a 1μs resolution. The data was then re-binned into appropriate time resolution. Data analysis was done using Origin 7.5 and LabVIEW (National Instruments).

Nucleosome samples were obtained from Dr Jonathan Widom, Northwestern University. Briefly, a 147-bp nucleosome positioning sequence (‘601’ sequence) which has a single dominant position was labeled with Cy3, the FRET donor at 5’ end. Recombinant *Xenopus laevis* histone octamer comprising of H2A, H2B, H3 (V35C C110A) and H4 were used to reconstitute the

nucleosomes. The FRET acceptor Cy5 was used to label H3 at the engineered cysteine residue.

Simulations: Monte Carlo simulations were carried out in Matlab (Mathworks) to simulate translation diffusion of molecules and kinetic transitions.. Monte Carlo simulations are powered by random sampling; however the random sampling must comply with a pre-described probability distribution. To simulate translation diffusion of fluorescent molecules, the following conditions are imposed. First, a sample box containing the confocal volume was created and its dimensions are sufficiently bigger than the confocal volume. The centers of the confocal volume and the sample box coincide at the coordinates (0,0,0). Then *N* molecules were randomly placed inside the box at time $t = 0$. Next, we choose the time resolution *dt* such that *dt* is smaller than the relevant time scales of the physical processes involved (diffusion and kinetics). After each step, the *N* molecules are displaced a certain distance *dr*, in a random direction, which is governed by translational diffusion coefficient *D* of the molecule(s) by the relation:

$$dr = (6Ddt)^{1/2} \tag{3-6}$$

The Cartesian coordinates for each molecule are then manipulated as follows:

$$\begin{aligned} x(t+dt) &= x(t) + \mathrm{dr}\cos(\varphi)\sin(\theta) \\ y(t+dt) &= y(t) + \mathrm{dr}\sin(\varphi)\sin(\theta) \\ z(t+dt) &= z(t) + \mathrm{dr}\cos(\theta) \end{aligned} \tag{3-7}$$

where the angles, θ and φ, are generated randomly using the limits $0 \leq \theta \leq \pi$ and $0 \leq \varphi \leq 2\pi$.

To simulate kinetics, molecules are allowed to interconvert between the states (of varying fluorescence signal for both donor and acceptor molecules). The rate at which the molecules interconvert is simulated as a probability *p* dictated by the kinetic rate *k*. For instance, if the rate of interconversion from state 1 to state 2 is k_{12} s^{-1}, then the probability that a molecule in state 1 will transition to state 2 in the time window *dt* is $p_{12} = k_{12}.dt$. Similarly the probability that a molecule in state 2 will convert to state 1 is $p_{21} = k_{21}.dt$. To attain dynamic equilibrium, the initial N molecules are separated into states 1 and 2 such that the ratio of molecules in the states is equal to the equilibrium constant $K = k_{12}/k_{21}$.

Finally, once the position and state of the molecules are determined, the fluorescence intensities are calculated by applying Gaussian illumination profile with the center at (0,0,0) and using r_0 and z_0, the radial and axial semiaxes of the observation volume. The donor intensity of each molecule is given by

$$I_D = J_{1,2} e^{-2(x^2+y^2)/w_1^2} e^{-2z^2/w_2^2} \quad \text{3-8}$$

and the acceptor intensity of each molecule is given by

$$I_A = K_{1,2} e^{-2(x^2+y^2)/w_1^2} e^{-2z^2/w_2^2} \quad \text{3-9}$$

where $J_{1,2}$ and $K_{1,2}$ are the donor and acceptor intensities of molecules in state 1 or 2 that is exactly at the center of the observation volume (0,0,0).

The total intensities in the donor and acceptor detectors are calculated as the sum of donor and acceptor intensity of the *N* molecules. This step is repeated for a total of *NN* cycles giving a total simulation time of *NN*dt*. The total intensity versus time results in the intensity traces which are then used to calculate the correlation functions. To get the correlation function of the proximity factor, the function $p(t)$ is first calculated and then correlated according to Eq. 3-4.

Results

To test the validity of the simulations, correlation functions obtained from simulations were fitted with established models. We ran simulations with one type of fluorescent species diffusing in a 3-dimensional Gaussian observation volume. The analytical expression for this condition has been solved and described in chapter 1 (Eq. 1-3) and shown again in Eq. 3-10. The results of the simulation are presented in Fig. 3-5 along with the fit to Eq. 1-3.

$$G_{diff}(\tau) = \frac{1}{\langle N \rangle} \cdot \frac{1}{1 + \frac{4D\tau}{r_0^2}} \cdot \frac{1}{\sqrt{1 + \frac{4D\tau}{z_0^2}}} \qquad 3-10$$

where D is the diffusion coefficient of the fluorophore, $\langle N \rangle$ is the mean number of molecules inside the confocal volume and r_0 and z_0 are the radial and axial axes of the confocal volume (Fig. 1-6). A good fit as seen in Fig. 3-5 indicates that the simulations are valid.

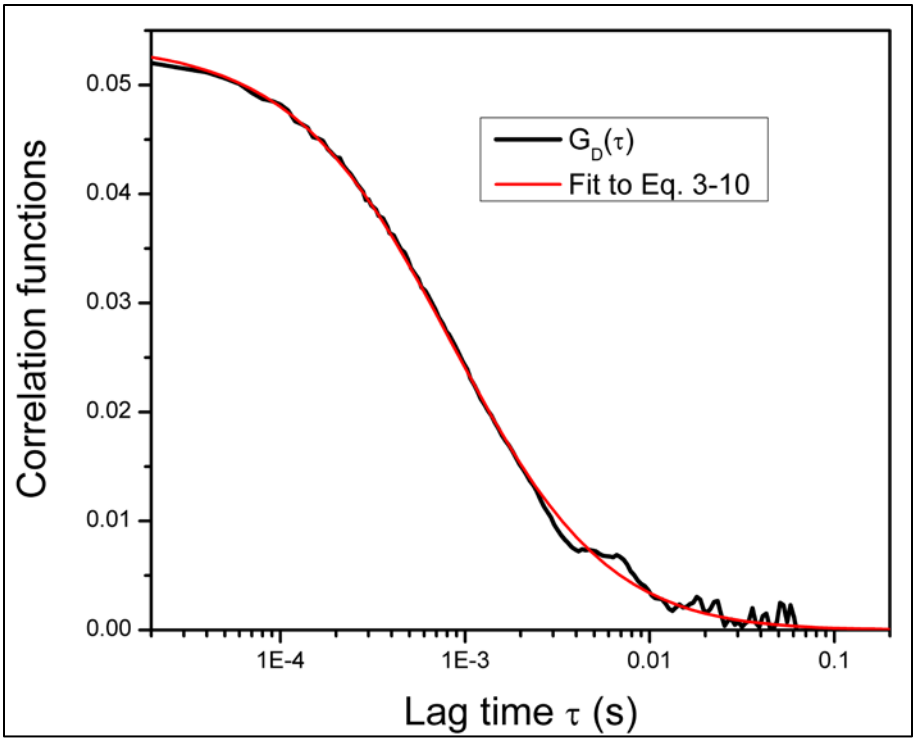

Fig. 3-5: Results of computer simulation for one type of fluorescent species. The black curve is the correlation of donor intensity ($G_D(\tau)$) and the red curve is a fit according to Eq. 3-10.

To validate the simulations with kinetic transitions, we ran simulations for a simple two-state mechanism. The resulting correlation of the donor intensity ($G_D(\tau)$) was divided by the diffusion contribution ($G_{Diff}(\tau)$ in Eq. 3-10) and the ratio was fit to an exponential decay according to Eq. 3-2. Fig. 3-6 shows the results of computer simulations for a system with two-state kinetic transitions. The ratio of the correlation of the donor intensity ($G_D(\tau)$) to the diffusion contribution ($G_{Diff}(\tau)$) is shown in black and it has been fitted to a kinetic model according to Eq. 3-2. This proves the validity of the simulations and further test conditions can now be simulated.

Let us consider a case where there is a system with just one species with proximity factor p_1. Now in an ideal case where there is no background, the signal in the acceptor and donor detector channels (S_A(t) and S_D(t) respectively) will be related by the equation

$$p_1 = \frac{S_A(t)}{S_A(t) + S_D(t)} \qquad 3\text{-}11$$

The function $p(t)$ will be a constant with values p_1 and hence the correlation function $G\mathrm{p}(t)$ will be zero. However, in reality, there is a background level in both detector channels. This leads to deviation of $p(t)$ from the mean value (p_1) and the fluctuations in p(t) are governed by diffusion. As molecules diffuse into the confocal volume, the value of p approaches p_1 while as the molecule diffuses out of the confocal volume, the value of p moves away from p_1 to background level.

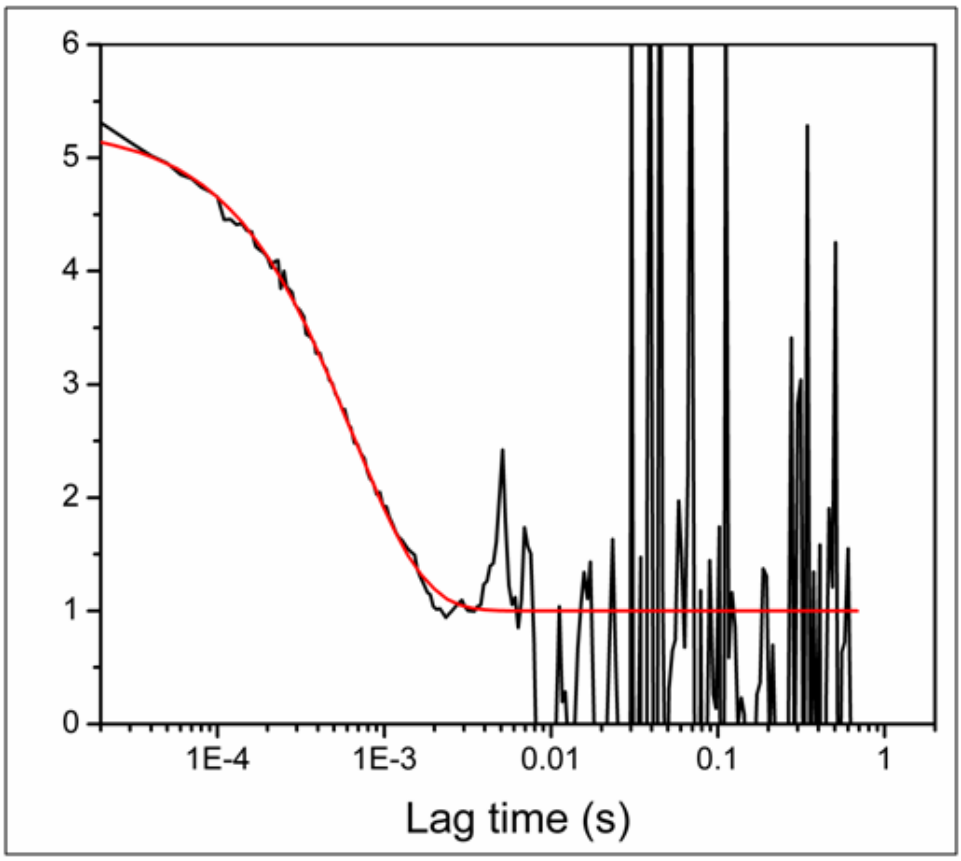

Fig. 3-6: Results of computer simulation for system with two-state kinetic transition. The black curve is the ratio of the correlation of donor intensity ($G_D(\tau)$) to the diffusion contribution ($G_{Diff}(\tau)$) (Eq. 3-10) and the red curve is a fit according to Eq. 3-2.

To test this, we ran simulations with just one population of molecules. The parameters chosen were N = 10000 molecules, sample box is a cube of dimension 6.4 μm, $r_0 = z_0$ = 0.35 μm (resulting in an average of ~9.1 molecules in the confocal volume). The simulation time resolution was set at dt = 1 μs and the diffusion coefficient of the molecule is 400 $\mu m^2/s$. J_1 and K_1 (the brightness of the molecule at the center of the confocal volume) were set at 4000 and 1000 (p_1 = 0.2). The total simulation time was 0.01s. Fig. 3-7 is the fluorescence intensity traces in the acceptor (red) and donor (black) channels. Calculating $p(t)$ from these intensity traces gives a constant value of 0.2 (p_1).

Background is simulated as random numbers following a Poisson distribution. The mean of the poisson distribution was kept at 5% of the mean fluorescence intensity in both channels. After addition of background, the proximity factor was calculated from the resulting intensity traces and its correlation function was calculated. Fig. 3-8 shows the correlation function of the proximity factor ($G_p(\tau)$) along with the correlation function of the donor intensity trace ($G_D(\tau)$).

From this example, we can see that even for a system with just one species and hence no kinetics, $G_p(\tau)$ clearly reflects diffusion when background is present. Note that since the total simulation time was 0.01 s, the correlation function of the proximity factor is very noisy. The noise can be reduced by increasing the simulation time. Hence from this simple demonstration, we can

show that the proximity factor correlation, $G_P(\tau)$ does not, in general, measure the relaxation time of the kinetic process (τ_R).

Now let us consider a system with two species of molecules, one with proximity factor p_1 and the other with proximity factor p_2 such that $0 \leq p_1 < p_2 \leq 1$. The molecules don't interconvert to each other ($k_{12} = k_{21} = 0$). Under these conditions, the confocal volume is occupied by a mixture of the two species and since the excitation volume is inhomogeneous, the fluorescence intensities in either donor or acceptor channel fluctuate depending on the relative concentrations of the two species and the proximity of either to the focal point of the observation volume.

Consequently, as molecules of higher *p* value diffuse towards the center of the confocal volume, the observed proximity factor approaches p_2 and while the molecules of lower *p* value diffuse towards the center of the confocal volume, the observed proximity factor approaches p_1. Hence, we predict, that the fluctuation in proximity factor depends on the diffusive properties of the species. To test this, we performed simulations with a solution containing a 50-50 mixture of two species of proximity factor 0.2 and 0.8. The rest of the parameters were maintained as before. The results of the simulations are presented in Fig. 3-9.

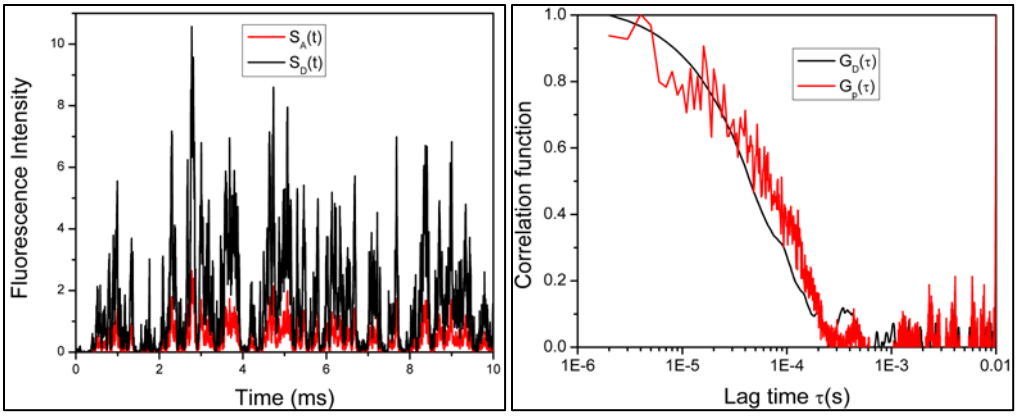

Fig. 3-7 (left): Fluorescence intenisty time traces for simulations without background. Intensities in the acceptor channel (red) and donor channel (black) fluctuate due to diffusion of molecules in and out of the confocal volume.

Fig. 3-8 (right): Results of a computer simulation for a one-species system with background set at 5% of signal. The red curve is the correlation of proximity factor ($G_P(\tau)$) and the black curve is the correlation of the donor intensity ($G_D(\tau)$).

As seen in Fig. 3-9, the correlation function of proximity factor ($G_P(\tau)$) overlaps with the correlation function of the fluorescence intensity in the donor channel ($G_D(\tau)$) thus proving our hypothesis correct. Note that in this simulation the diffusion coefficients of the two species were kept the same and thus $G_D(\tau)$ (and $G_P(\tau)$) can be fit with a single species model. If the diffusion coefficients were significantly different, both functions would have to be fit with a two species model.

Now this argument can be extended to a case where the kinetic timescale is much slower than the diffusion timescale ($\tau_R >> \tau_D$). Here, the molecules interconvert much slower than their diffusion time and so they enter and pass through the confocal volume in just one state. Hence the system appears as a static system with no interconversion between the two states during the transit time. This condition can be simulated by using the same conditions as before, this time adding kinetics. The average residence time of the molecules τ_D can be calculated by using the formula $\tau_D = r_0^2/4D$. For a diffusion coefficient of 400 $\mu m^2/s$ and $r_0 = 0.35$ μm, the diffusion time is ~75 μs. We ran simulations with τ_R = 1ms such that $\tau_R >> \tau_D$. The rest of the parameters were maintained as before. For simplicity, the rates of interconversion were kept equal $k_{12} = k_{21} = 500\ s^{-1}$ and hence $\tau_R = (k_{12}+k_{21})^{-1}$ = 1ms. Hence in the simulation, the probability of interconversion in a time window dt was $p_{12} = p_{21} = k_{12}.dt = 5*10^{-4}$. The total simulation time was 0.01 s ($1*10^4$ cycles). The results of the simulations are

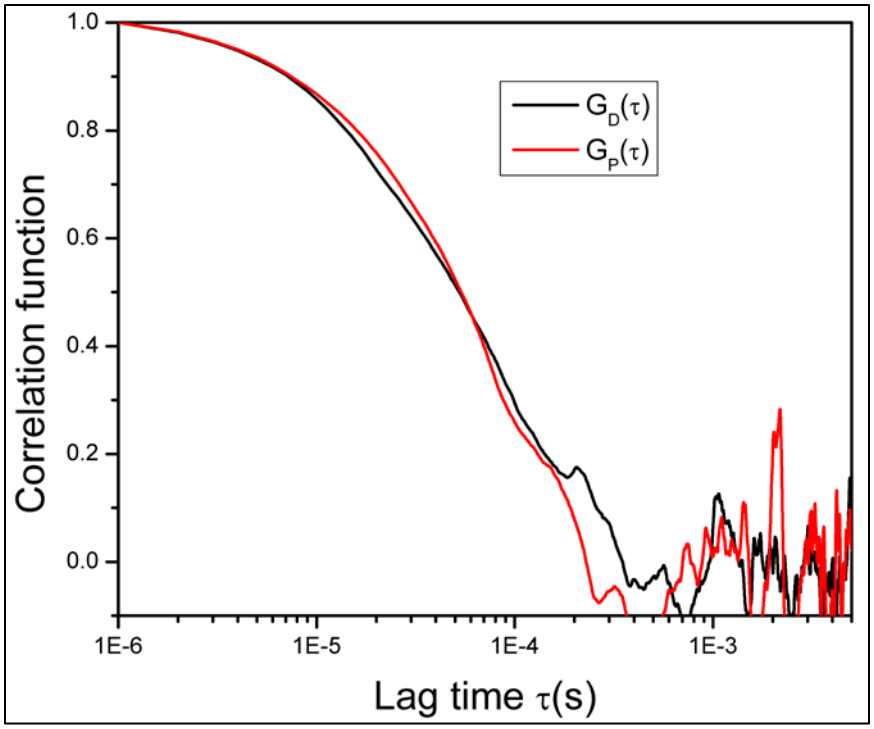

Fig. 3-9: Results of a computer simulation for a two-species system with no interconversion. The red curve is the correlation of proximity factor ($G_P(\tau)$) and the black curve is the correlation of the donor intensity ($G_D(\tau)$). The overlap between the two proves that the correlation of proximity factor has contributions from diffusion.

shown in Fig. 3-10. The correlation function of the proximity factor, $G_P(\tau)$, clearly overlaps with the correlation function of the donor channel fluorescence intensity $G_D(\tau)$ and it decays much faster than 1 ms (kinetic relaxation time set in the simulation.

Our motivation to pursue the simulations was directed towards recovering the timescales of conformation dynamics of nucleosomes. From previous results, it was known that the conformational dynamics of nucleosomes occur at ~50 ms [4,11] and for a typical confocal setup the residence time of a nucleosome is 1-10ms. Hence, these conditions clearly follow the $\tau_R > \tau_D$ regime and the correlation function of the proximity factor reflects diffusion timescales rather than kinetic timescales. Fig. 3-11 shows the experimental correlation curves obtained with nucleosomes.

Comparing Fig. 3-10 and 3-11, we can see that for the $\tau_R > \tau_D$ regime, the correlation function of the proximity factor has significant contribution from diffusion and cannot yield kinetic timescales.

Simulations were also performed for the conditions where the kinetic relaxation timescale was kept close to the diffusion time. The parameters used were τ_R = 250 μs and τ_D = 150 μs. The rest of the simulation parameters were repeated as prescribed before. The results of the simulations are presented in Fig. 3-12.

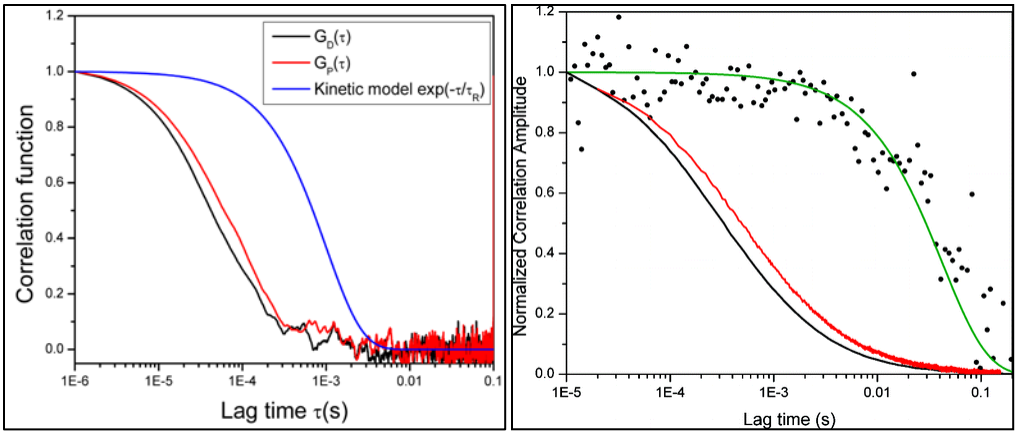

Fig. 3-10 (left): Results of a computer simulation with parameters τ_R = 1 ms and τ_D = 75 μs. The red curve is the correlation of proximity factor ($G_P(\tau)$) and the black curve is the correlation of the donor intensity ($G_D(\tau)$) . The blue curve is a two-state kinetic model with a relaxation time of 1 ms fit according to Eq. 3-2.

Fig. 3-11 (right): Experimental correlation curves obtained with nucleosomes. The black dots represent the ratio of the donor autocorrelation functions of donor−acceptor and donor-only nucleosomes following the methodology used by Bonnet et al. [10] and the green curve is a fit to a two-state model with a relaxation time of 50 ms. The black curve is the autocorrelation of the donor intensity ($G_D(\tau)$), which represents the diffusion contributions and the red curve is the correlation of the proximity factor ($G_P(\tau)$).

Finally, for the case where the relaxation occurs faster than diffusion ($\tau_R << \tau_D$), the correlation of the proximity factor represents the relaxation times and has no contribution from diffusion. Under these conditions, the confocal volume is occupied by molecules of high and low proximity factors. Since the relaxation time is much lower than the residence time, each of the molecules undergo multiple transitions between high and low proximity factor states before exiting the confocal volume. Hence the fluctuations in proximity factor are governed by kinetics rather than diffusion. To test this prediction, we performed a simulation with τ_R =100 μs and τ_D = 1ms. The rest of the parameters were maintained as before. Results of the simulation are shown in Fig. 3-13. Under the conditions where diffusion is slower than kinetics ($\tau_R << \tau_D$), the proximity factor correlation yields kinetic timescales and has no contribution from diffusion.

From the above discussion, we have shown that proximity factor correlation can have significant contributions from diffusion under cases where diffusion is faster than kinetics or with similar timescales ($\tau_R >> \tau_D$ or $\tau_R \sim \tau_D$). Only in cases where the kinetics is much faster than diffusion ($\tau_R << \tau_D$), the proximity factor correlation is free of contributions from diffusion.

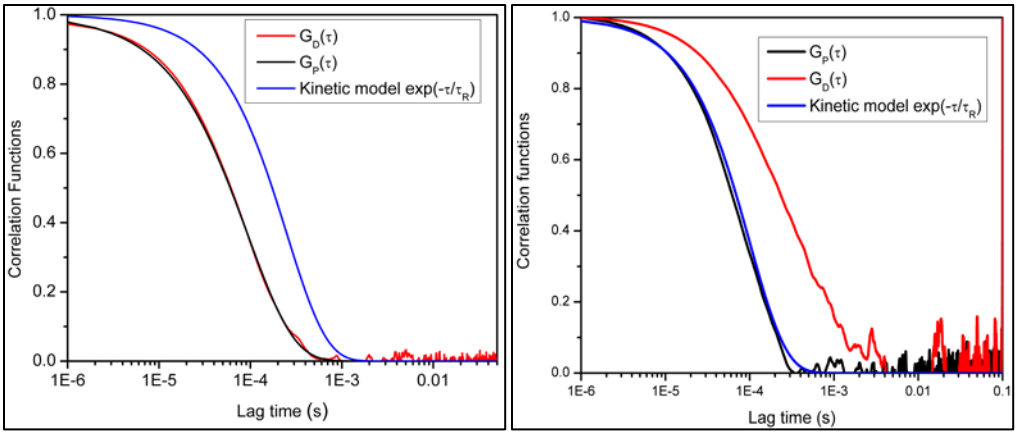

Fig. 3-12 (left): Results of a computer simulation with parameters τ_R = 250 μs and τ_D = 150 μs. The black curve is the correlation of proximity factor ($G_P(\tau)$) and the red curve is the correlation of the donor intensity ($G_D(\tau)$) . The blue curve is a two-state kinetic model with a relaxation time of 250 μs fit according to Eq. 3-2.

Fig. 3-13 (right): Results of a computer simulation with parameters τ_R = 100 μs and τ_D = 1 ms. The black curve is the correlation of proximity factor ($G_P(\tau)$) and the red curve is the correlation of the donor intensity ($G_D(\tau)$) . The blue curve is a two-state kinetic model with a relaxation time of 100 μs fit according to Eq. 3-2.

Discussion

Klenerman et al. used the proximity factor correlation to recover the timescales of kinetic processes[14,15]. After obtaining the proximity factor correlation, they used a stretch-parameter exponential function to fit the correlation function and obtain the kinetic timescales. The stretch parameter is usually interpreted as the deviation from a simple two-state mechanism. If a system undergoes simple two-state kinetic transitions, the stretch parameter is close to 1, while a value of $\beta < 1$ implies multiple intermediates. Klenerman's group used this methodology to study DNA hairpins and obtained β values close to 0.5 and kinetic relaxation time (τ_R) of 150 – 350 μs (which is very close to the diffusion timescale for this system) and suggested that DNA hairpins do not follow two-state kinetic transitions. This interpretation was in disagreement with previous results obtained with DNA haipins using FCS[10] and laser T-jump experiments[16-18] that had in fact proved that hairpin kinetics follow a two-state mechanism. In fact, the correlation of donor intensity obtained for a one-species system can be fit with a stretched-parameter model. This fit is presented in Fig 3-14 and we can see that FCS decay with only diffusion contribution can be successfully fitted with a stretched-parameter model.

With the results shown above, it is highly likely that the proximity factor correlation obtained by Klenerman et al. is contaminated with contributions from translational diffusion and does not directly reflect kinetic transitions. Hence, the

application of proximity factor correlation to studying conformational dynamics has to be done by taking a lot of factors into consideration. Only in cases where diffusion is much slower than kinetics, the proximity factor correlation is free of contributions from diffusion, in all other cases; diffusion contributes to proximity factor correlation. Imposing an incorrect model (like the stretch-parameter model) on the experimental results can lead to erroneous understanding of the system.

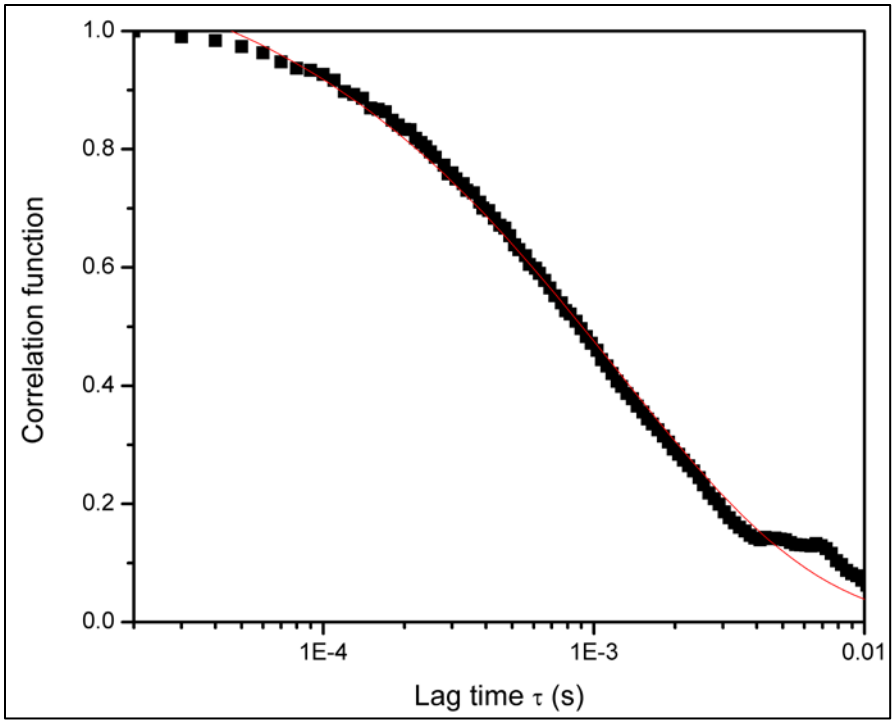

Fig. 3-14: Results of computer simulation for one species system with τ_D = 1ms. The black dots are the correlation of donor intensity ($G_D(\tau)$) and the red is a fit according to Eq. 3-5 with τ_R = 1 ms and β = 0.5.

References

(1) Widengren, J.; Mets, U.; Rigler, R. *J. Phys. Chem.* **1995**, *99*, 13368-13379.

(2) Widengren, J.; Schwille, P. *J. Phys. Chem. A* **2000**, *104*, 6416-6428.

(3) Icenogle, R. D.; Elson, E. L. *Biopolymers* **1983**, *22*, 1919-1948.

(4) Li, G.; Levitus, M.; Bustamante, C.; Widom, J. *Nat. Struct. Mol. Biol.* **2005**, *12*, 46-53.

(5) Edman, L.; Mets, U.; Rigler, R. *Proc Natl Acad Sci USA* **1996**, *93*, 6710-6715.

(6) Chattopadhyay, K.; Saffarian, S.; Elson, E. L.; Frieden, C. *Proc Natl Acad Sci USA* **2002**, *99*, 14171-14176.

(7) Kim, H. D.; Nienhaus, G. U.; Ha, T.; Orr, J. W.; Williamson, J. R.; Chu, S. *Proc Natl Acad Sci USA* **2002**, *99*, 4284-4289.

(8) Talaga, D. S.; Lau, W. L.; Roder, H.; Tang, J. Y.; Jia, Y. W.; DeGrado, W. F.; Hochstrasser, R. M. *Proc Natl Acad Sci USA* **2000**, *97*, 13021-13026.

(9) Cosa, G.; Harbron, E. J.; Zeng, Y. N.; Liu, H. W.; O'Connor, D. B.; Eta-Hosokawa, C.; Musier-Forsyth, K.; Barbara, P. F. *Biophys. J.* **2004**, *87*, 2759-2767.

(10) Bonnet, G.; Krichevsky, O.; Libchaber, A. *Proc Natl Acad Sci USA* **1998**, *95*, 8602-8606.

(11) Torres, T.; Levitus, M. *J. Phys. Chem. B* **2007**, *111*, 7392-7400.

(12) Poirier, M. G.; Oh, E.; Tims, H. S.; Widom, J. *Nat. Struct. Mol. Biol.* **2009**, *16*, 938-U59.

(13) Egele, C.; Schaub, E.; Piemont, E.; de Rocquigny, H.; Mely, Y. *C. R. Biol.* **2005**, *328*, 1041-1051.

(14) Wallace, M. I.; Ying, L. M.; Balasubramanian, S.; Klenerman, D. *J. Phys. Chem. B* **2000**, *104*, 11551-11555.

(15) Wallace, M. I.; Ying, L. M.; Balasubramanian, S.; Klenerman, D. *Proc Natl Acad Sci USA* **2001**, *98*, 5584-5589.

(16) Ansari, A.; Kuznetsov, S. V. *J. Phys. Chem. B* **2005**, *109*, 12982-12989.

(17) Ansari, A.; Kuznetsov, S. V.; Shen, Y. Q. *Proc Natl Acad Sci USA* **2001**, *98*, 7771-7776.

(18) Shen, Y. Q.; Kuznetsov, S. V.; Ansari, A. *J. Phys. Chem. B* **2001**, *105*, 12202-12211.

Chapter 4

NUCLEOSOME DISASSEMBLY PATHWAY: A DUAL COLOR FLUORESCENCE CROSS-CORRELATION SPECTRSCOPY STUDY

Introduction

Nucleosomes are transient protein-DNA complexes and are often undergoing conformational dynamics to allow regulatory proteins to bind to their target site. It is very important to understand the mechanism undertaken during nucleosome conformational changes to study DNA metabolic pathways. Nucleosomes sterically hinder the binding of these enzymes and hence their conformational dynamics play an important role in gene regulation[1]. Various models are used to represent the conformational changes in nucleosomes including nucleosome repositioning, transient DNA unwrapping/rewrapping and exchange of histone proteins. Li et al. used stopped-flow FRET measurements along with Fluorescence correlation spectroscopy (FCS) to measure the kinetic rates of DNA unwrapping and rewrapping onto nucleosomes[2]. Detailed studies of histone protein release and exchange have not been done.

In various *in vitro* experiments, the ionic strength of the buffer is modulated to alter the electrostatic interactions between the DNA and the proteins in the nucleosomes. *In vitro* nucleosome assembly is performed by placing the DNA and the histone proteins in a buffer with high NaCl concentration and by using a step-wise dialysis to reduce the salt concentration to physiological

conditions[3]. In fact, if the DNA and the histone proteins are mixed at physiological conditions, they form insoluble aggregates and do not reconstitute into nucleosomes. This indicates that although the formation of nucleosomes is thermodynamically favorable, there is a kinetic barrier for its formation. The ionic strength, at high salt concentration, allows the barrier to be crossed and form stable nucleosomes.

In a similar fashion, when the ionic strength is increased, nucleosomes are disassembled. The precise mechanism of this disassembly is not known[4]. One model predicts a step wise disassembly of the proteins[5-8] (shown in Fig. 4-1) while another model predicts that the whole protein octamer is lost from the nucleosomes in one step[9] (shown in Fig. 4-2). Many groups have attempted to study the disassembly intermediates, mostly using Förster Resonance Energy Transfer (FRET) at a single molecule level[4,10,11]. Although the technique of single molecule FRET has its strengths[12], the caveat is that it requires really low concentrations (< 50 picomolar). Especially in the case of nucleosomes, it has been shown before that under these extreme concentration conditions, nucleosomes are unstable and fall apart[13]. Hence the results of these experiments have to be further verified.

In this chapter, we present our experiments using dual color Fluorescence Cross-Correlation Spectroscopy (FCCS) to study nucleosome disassembly pathway induced by changing the ionic strength. FCCS measures the concomitant

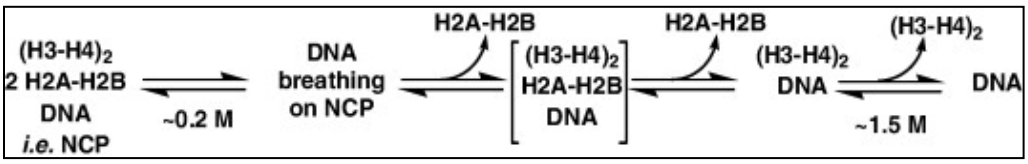

Fig.4-1: Model for stepwise disassembly of nucleosomes. As NaCl concentrations are increased, The H2A-H2B dimers dissociate are released at ~0.4M NaCl. The $(H3\text{-}H4)_2$ tetramer then dissociates above 1.4M NaCl. Reprinted [8] with permission.

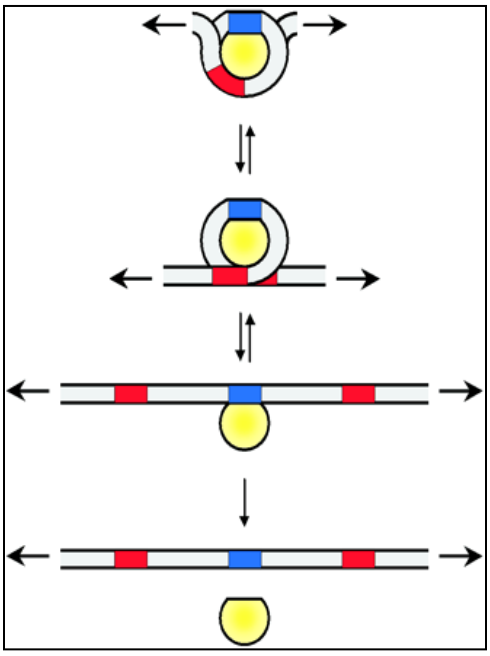

Fig.4-2: Model for one-step disassembly of nucleosomes. Nucleosomes are disassembled by removing the protein core in one step. Reprinted [9] with permission

diffusion of two fluorophores (or fluorophore tagged biomolecules) and are often used to study colocalization and binding. By performing FCCS experiments on nucleosomes with one dye on the DNA and the other dye on a histone protein, we can study the binding between the DNA and every individual histone protein. Preliminary results indicate that nucleosomes undergo disassembly upon increasing the ionic strength by addition of salt. However, to arrive at a quantitative model, further experiments need to be performed.

Dual color Fluorescence Cross-Correlation Spectroscopy

Fluorescence correlation spectroscopy (FCS) is a technique based on the temporal fluctuations in the fluorescence intensities. FCS applications analyze the diffusion and kinetic properties of fluorophores (or fluorescently labeled molecules). However, dual color Fluorescence Cross-Correlation Spectroscopy (FCCS) can reveal information about the concomitant diffusion of two spectrally distinguishable fluorophores[14]. Here, the two fluorescent probes are excited simultaneously by two different light sources and their fluorescence is detected by two independent detectors. The confocal observation volume is created by overlapping the two light beams. Only when molecules containing both the fluorescent probes diffuse through the observation volume, FCCS signal is detected. Differences between FCS and FCCS are illustrated in Fig. 4-3.

For example, a double-stranded DNA substrate was labeled with a red (Cy5) and green (Rhodamine green) dye at opposite ends and the restriction

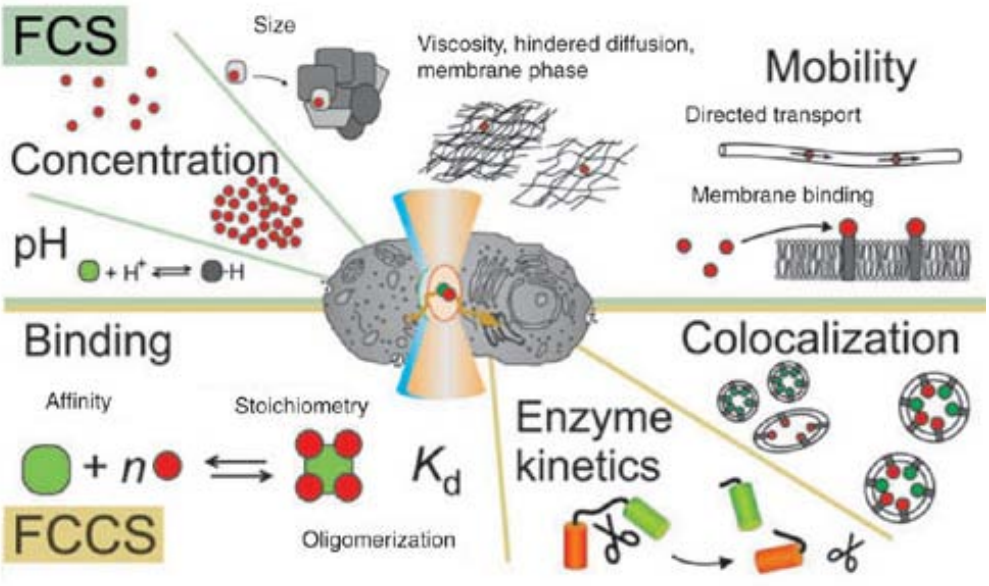

Fig. 4-3: Differences between FCS and FCCS measurements. FCS measures fluctuations in concentration via diffusion and other physical processes and yields timescales of these processes. FCCS measures binding and colocalization. Reprinted [17] with permission.

endonuclease *E*coRI was added to cleave the DNA at an internal site. Due to the site specific breaks induced by *Eco*RI, the number of doubly-labeled DNA substrate molecules decreased successively with the enzyme reaction progress. Enzyme activity down to 1 pM was determined successfully by monitoring the cross-correlation function[15] (Fig. 4-4).

The normalized cross-correlation function, $G_c(\tau)$, is calculated as a time average of the product of the fluctuations in the two fluorescence intensities I_a and I_b. Here I_a and I_b are the intensities recorded in the two detectors. It is defined as

$$G_C(\tau) = \frac{\langle \delta I_a(t) \delta I_b(t+\tau) \rangle}{\langle I_a(t) \rangle \langle I_b(t) \rangle} \quad 4\text{-}1$$

where $\delta I(t)$ represents the fluctuations in the fluorescence intensity $I(t)$ defined as

$$\delta I(t) = I(t) - \langle I(t) \rangle \quad 4\text{-}2$$

where $\langle I(t) \rangle$ is the mean fluorescence intensity.

FCCS has also been successfully demonstrated in living cells to study endocytic pathways[16,17]. Many commercial systems are being developed to perform FCCS.

When performing FCCS measurements, special considerations to cross-talk, and fluorescence resonance energy transfer (FRET) must be provided, which in many cases require additional data processing to prevent false positive signals arising from spectral leakage and to improve data quality[18]. This cross-talk (signal leakages into other detection channel) is typically a result of the overlap between

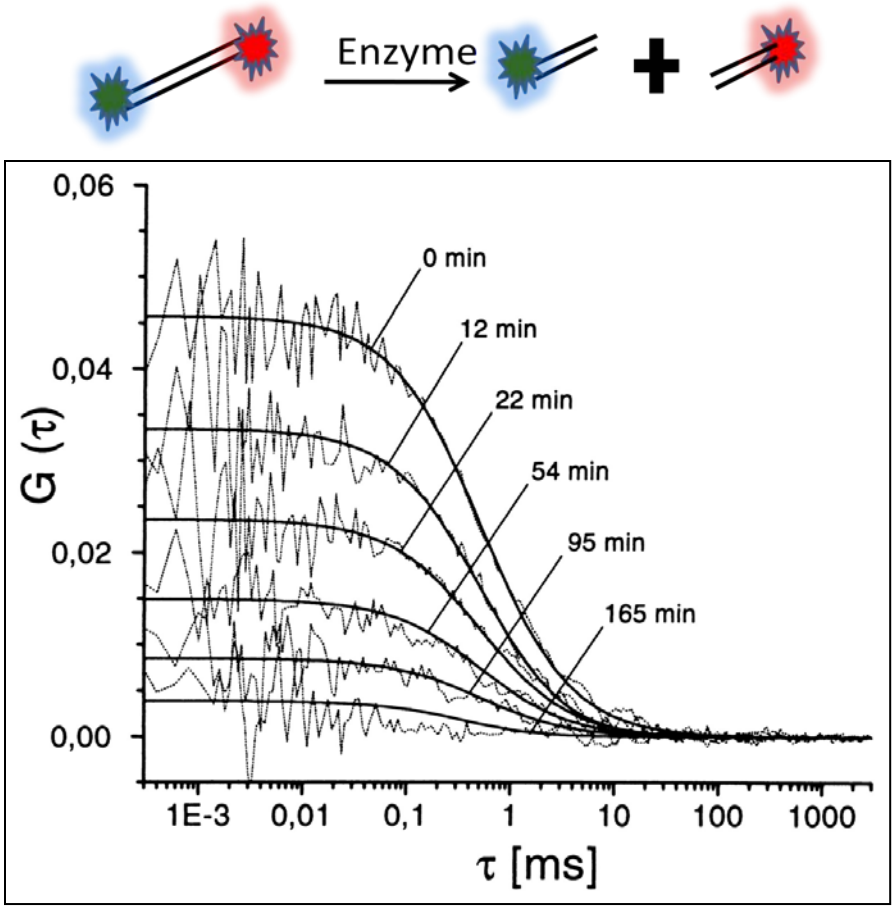

Fig. 4-4: Top: Double stranded DNA was labeled at two ends with two dyes. Restriction enzyme was used to cleave the DNA into two parts, each with one dye. Only molecules with both dyes contribute to FCCS. Bottom: Experimental FCCS curves. Cleavage reaction of the enzyme *Eco*RI was monitored at different time points. The DNA substrate was labeled with Cy5 and Rhodamine Green at opposite ends. As the enzymatic reaction was carried out, the DNA substrate was cleaved resulting in a loss of cross-correlation amplitude. Reprinted [15] with permission.

the emission spectra of the two fluorophores. To solve these issues, new methodologies such as single laser wavelength FCCS (SW-FCCS),[19] two-photon excitation (TPE),[20] and grating-based four-color FCCS using quantum dots, have been proposed[21]. For example, Hwang *et al*. proposed SW-FCCS using a single excitation (TPE),[20] and grating-based four-color FCCS using quantum dots, have been proposed[21]. For example, Hwang *et al*. proposed SW-FCCS using a single laser excitation beam at 488 nm to excite a combination of labels emitting at 510 nm and 695 nm with different Stokes shifts[19]. However, cross-talk was not completely suppressed. Thews *et al*. successfully eliminated cross-talk signals in their FCCS measurements by adopting an acousto-optic modulator (AOM)-based pulse picker system to make alternating laser beams of different colors (a blue laser at 425 nm and a green laser at 515 nm)[22]. The emitted photons of two different fluorophores were counted using a single detector, which was synchronized with the AOM system.

Materials and Methods

Nucleosome samples

The nucleosome samples used were the same as described in Chapter 2. Samples DA1, DA35 and DA57 were used for FCCS experiments. DA1 sample consisted of Cy3 labeled at position 1 of the "601" nucleosome positioning sequence[23] while Cy5 was attached to an engineered cysteine on the H3 histone protein (H3 V35C). DA35 sample consisted of Cy3 labeled at position 35 of the

"601" nucleosome positioning sequence while Cy5 was attached to an engineered cysteine on the H2B histone protein (H2B T112C). DA57sample consisted of Cy3 labeled at position 57 of the "601" nucleosome positioning sequence while Cy5 was attached to an engineered cysteine on the H4 histone protein (H4 L22C). Since FCCS recognizes the concomitant diffusion of the fluorophores, it can be used to detect whether the nucleosomal DNA is in contact with the individual histone proteins H2B, H3 and H4. All nucleosome samples were prepared in the Widom lab, Northwestern University.

Fluorescence Cross-Correlation Spectroscopy

FCCS experiments were carried out in a home-built confocal setup. This setup is a modification of the one described in Chapter 2. For excitation, a 532 nm CW laser from Coherent (215M-10, Coherent Inc., Santa Clara, CA) and a 640 nm CW laser from Coherent (Cube 640-40, Coherent Inc., Santa Clara, CA) were overlapped using a dichroic mirror. This dichroic mirror reflects the red laser and transmits the green laser. An additional filter (Semrock Filter LD01-640/8-12.5) was used to clean the output of the red laser. The two lasers were independently expanded and collimated to a Gaussian beam profile using a pair of lenses. The lenses were chosen such that the expanded laser beam just filled the back aperture of the objective (Olympus Plan Apo 100X 1.4NA). Positioning the second lens on a two-axis stage (Newport 460A series) permitted fine tuning of the size of the beam and its collimation The laser power was attenuated to the desired power

using neutral density filters. A pair of two-axis mirrors was used to steer the beam and the laser is then directed onto a 45^0 dichroic mirror (Semrock Filters FF545/650-Di01). The dichroic mirror was used to reflect the two lasers while transmitting the fluorescence emitted by both dyes. The reflected beam entered the back aperture of the Olympus objective and focused to a diffraction limited spot in the sample. The sample was mounted on a dry clean glass coverslip (Fisher Scientific #1.5) within a perfusion chamber (Grace Biolabs PC8R-0.5). The objective assembly was housed on an optical stage (Thorlabs) and the objective position is adjusted using a micrometer of 750 nm resolution. Fluorescence emission from the sample was collected by the same objective lens and passed through the primary dichroic mirror. The fluorescence emission was then passed through a lens of known focal length and focused onto a pinhole (50 µm) which is positioned at the conjugate image plane of the focusing lens. The whole pinhole assembly was mounted on a cage system (Thorlabs) and supported by heavy posts to minimize the drift and to maintain collinearity. The light coming out of the pinhole was then collimated again using a second lens and then was split into two beam paths using a second dichroic mirror (Semrock Filters FF662-FDi01). The two beam paths belong to the FRET donor (Cy3) and FRET acceptor (Cy5) respectively. The light beams were then steered using a pair of two-axis mirrors and focused on the sensitive area of a single-photon counting module, (SPCM-AQR-14, Perkin Elmer). Additional optical filters (Omega

optical 3rd generation filters 3RD560-620 and 3RD670-740 for Cy3 and Cy5) were used to minimize background in either channel. The detector output is collected by a multi-tau digital hardware correlator (ALV-5000, ALV Gmbh) for cross-correlation traces.

All experiments were performed with 10 nM donor-acceptor nucleosome samples in 1 X TE buffer in the presence of 100 nM unlabeled nucleosome core particles to decrease the likelihood of nucleosome dissociation.

Results

Fluorescence Cross-Correlation Spectroscopy (FCCS) was performed on all three nucleosome samples: DA1, DA35 and DA57. As mentioned in Chapter 2, when the nucleosomes are in the wrapped conformation, there is high FRET efficiency ($E \sim 1.0$) in all nucleosome samples. This contributes to high brightness in the Cy5 detector channel not arising from direct excitation. To circumvent this issue, the red laser power was increased so as to maintain a higher brightness in the Cy5 detector channel from direct excitation. The brightness in each detector channel arising from different sources is summarized below in Table 4-1.

Table 4-1: Brightness (counts per ms) in detector channels from different sources at 0 M NaCl

Detector Channel	Cy3	Cy5
Background	1.5	2.1
Direct excitation	60	300
Crosstalk	~ 0	6
Cross-excitation	~ 0	10
FRET	~ 0	40

As seen from Table 4-1, the brightness in the Cy3 channel was completely due to direct excitation of the fluorophore by the green laser. However, the brightness in the Cy5 channel was a sum of brightness due to direct excitation, crosstalk, cross-excitation (excitation of Cy5 by green laser) and FRET. In FCS, the autocorrelation function for a multicomponent system is given by

$$G(\tau) = \frac{\sum_i N_i B_i^2 g_i(\tau)}{(\sum_i N_i B_i)^2} \qquad 4\text{-}3$$

where N_i is the number of molecules with brightness B_i and correlation decay $g_i(\tau)$.$g_i(\tau)$ represents just the shape of the decay and hence is normalized so that $g_i(0) = 1$.

Similarly in FCCS, the cross-correlation function is given by

$$G_C(\tau) = \frac{\sum_i N_i B_{i,a} B_{i,b} g_{i,C}(\tau)}{\sum_i N_i B_{i,a} \sum_i N_i B_{i,b}} \qquad 4\text{-}4$$

where $B_{i,a}$ and $B_{i,b}$ represent the brightness of the species *i* in the two detectors. To keep the contribution of FRET and cross-talk to the overall cross-correlation amplitude at a minimum, the brightness in Cy5 detector due to direct excitation was maintained high. As NaCl concentration was increased, the FRET efficiency decreased due to disassembly of the nucleosomes and this further decreased the brightness in the Cy5 channel due to FRET.

As the ionic strength was increased by the addition of NaCl, the electrostatic interactions between the positively charged histone proteins and the negatively charged DNA is screened leading to disassembly. This eventually leads to the loss of binding between the histone proteins and the DNA. As the population of intact nucleosomes with both dyes decrease, the amplitude of the FCCS curves decreased. As seen in Fig. 4-5, 4-6 and 4-7, for all nucleosome samples, DA1, DA35, and DA57, showed a decrease in the amplitude of the FCCS curves indicative of disassembly.

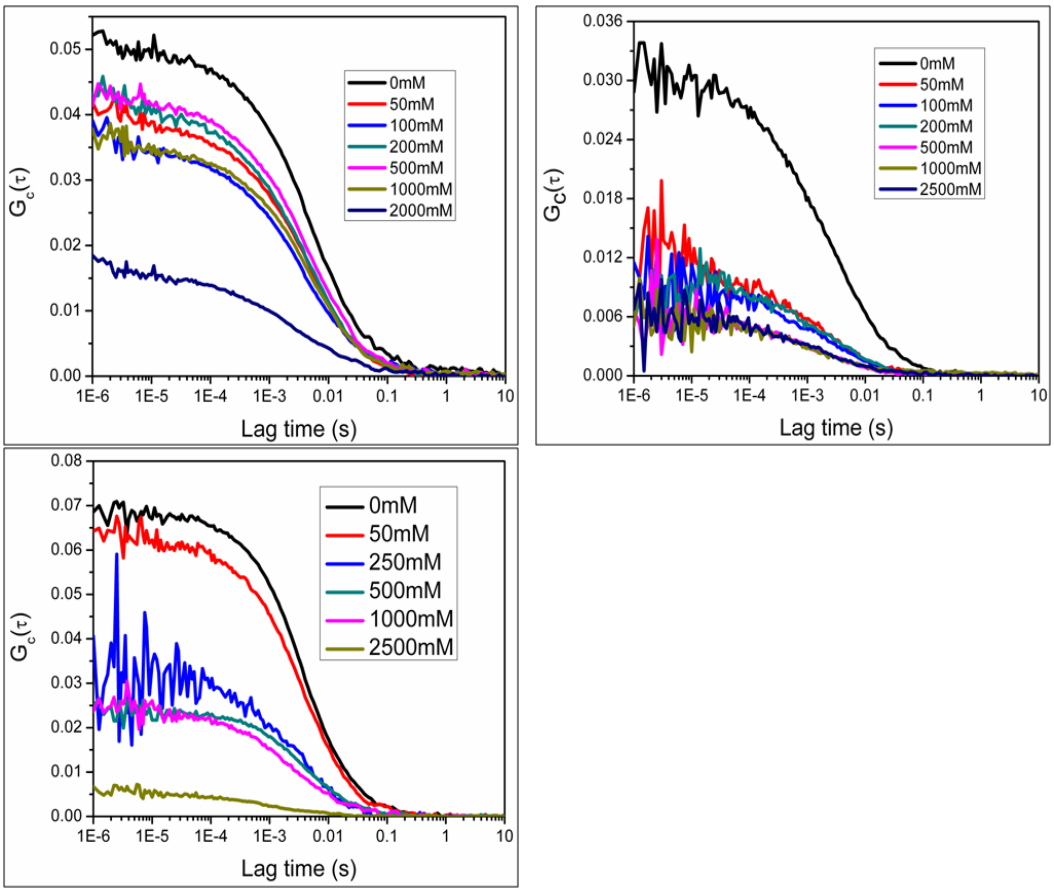

Fig. 4-5 (top left), 4-6 (top right) and4-7 (bottom): FCCS curves for DA1, DA35 and DA47. As NaCl concentration was increased from 0mM to 2000mM, the amplitude of the cross-correlation decreased.

Discussion

Nucleosome disassembly intermediates were studied using dual color Fluorescence Cross-correlation Spectroscopy (FCCS). FCCS experiments monitor the concomitant diffusion of two fluorophores and are applicable to study binding. By labeling the nucleosome DNA with the fluorescent dye Cy3 and labeling different histone proteins individually with the fluorescent dye Cy5, binding affinity between different histone proteins and the DNA was probed. For nucleosome sample DA1, Cy3 was attached to the DNA while Cy5 was attached to the histone protein DA1. Similarly, for samples DA35 and DA57, Cy3 was attached to the DNA while Cy5 was attached the histone proteins H2B and H4 respectively. By performing FCCS experiments on sample DA1 and DA57; we probed the binding between the DNA and $(H3\text{-}H4)_2$ tetramer, while by performing FCCS experiments on the DA35 sample; we probed the binding between the DNA and H2A-H2B dimer.

Ionic strength was modulated by the addition of NaCl and this in turn led the screening of the electrostatic interactions between the DNA and the histone proteins. This initiated the disassembly process and consequently led to the separation of the fluorophores. This was detected by observing the amplitude of the FCCS curves with various salt concentrations.

All nucleosome samples showed a decrease in the FCCS amplitude upon addition of NaCl. This is consistent with the hypothesis that increasing the ionic

strength of the solutions leads to disassembly of the nucleosomes by screeing the interactions between the DNA and the histone proteins. However, a quantitative model cannot be concluded from the current set of data. The exact intermediates in the nucleosomes disassembly pathway cannot be pinpointed. The experiments have to be repeated to get further insight into the disassembly pathway.

Another alternative method to probe the disassembly intermediates is by probing the Cy5 labeled molecules using the red laser. The dye Cy5 was used to label the histone proteins and when the nucleosomes undergo disassembly, there is a huge shift in the molecular weight of Cy5 labeled molecules (Fig. 4-8). The whole intact nucleosome is 210 kDa in size; however the individual histone proteins are 11-15 kDa depending on the histone protein. This change in molecular weight can alter the diffusion time of the Cy5 labeled molecules. By using the red laser to measure the autocorrelation of Cy5 labeled molecules for each nucleosome sample, we can monitor the size of the Cy5 labeled molecules and study the intermediates in nucleosome disassembly.

To summarize, FCCS and FCS experiments will be used to characterize the intermediates in nucleosome disassembly pathway. A better understanding of the nucleosome disassembly pathway and other conformational changes in nucleosomes is essential to understand regulation of gene expression.

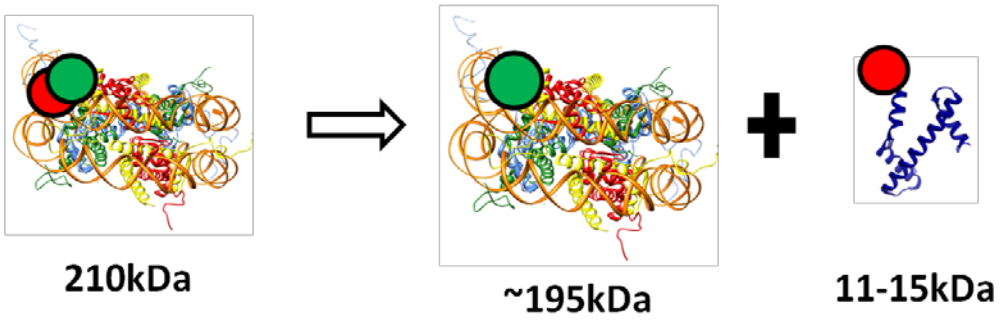

Fig. 4-8: Nucleosome disassembly particles. Cy3 (green circles) and Cy5 (red circles) are used to label the nucleosomes. Upon disassembly, the Cy3 labeled species separate from the Cy5 labeled species. As shown here, there is considerable decrease in the molecular weight of Cy5 labeled molecules and this can identified using autocorrelation of Cy5 under red laser illumination.

Reference

(1) Kornberg, R. D.; Lorch, Y. *Cell* **1999**, *98*, 285-94.

(2) Li, G.; Levitus, M.; Bustamante, C.; Widom, J. *Nat Struct Mol Biol* **2005**, *12*, 46-53.

(3) Wilhelm, F. X.; Wilhelm, M. L.; Erard, M.; Duane, M. P. *Nucleic Acids Res* **1978**, *5*, 505-21.

(4) Bohm, V.; Hieb, A. R.; Andrews, A. J.; Gansen, A.; Rocker, A.; Toth, K.; Luger, K.; Langowski, J. *Nucleic Acids Res*.

(5) Oohara, I.; Wada, A. *J Mol Biol* **1987**, *196*, 399-411.

(6) Park, Y. J.; Dyer, P. N.; Tremethick, D. J.; Luger, K. *J Biol Chem* **2004**, *279*, 24274-82.

(7) Teif, V. B.; Rippe, K. *Nucleic Acids Res* **2009**, *37*, 5641-55.

(8) Hoch, D. A.; Stratton, J. J.; Gloss, L. M. *J Mol Biol* **2007**, *371*, 971-88.

(9) Brower-Toland, B. D.; Smith, C. L.; Yeh, R. C.; Lis, J. T.; Peterson, C. L.; Wang, M. D. *Proc Natl Acad Sci U S A* **2002**, *99*, 1960-5.

(10) Gansen, A.; Valeri, A.; Hauger, F.; Felekyan, S.; Kalinin, S.; Toth, K.; Langowski, J.; Seidel, C. A. *Proc Natl Acad Sci U S A* **2009**, *106*, 15308-13.

(11) Koopmans, W. J.; Buning, R.; Schmidt, T.; van Noort, J. *Biophys J* **2009**, *97*, 195-204.

(12) Ha, T. *Methods* **2001**, *25*, 78-86.

(13) Kelbauskas, L.; Chan, N.; Bash, R.; Yodh, J.; Woodbury, N.; Lohr, D. *Biochemistry* **2007**, *46*, 2239-48.

(14) Schwille, P.; Meyer-Almes, F. J.; Rigler, R. *Biophys. J.* **1997**, *72*, 1878-86.

(15) Kettling, U.; Koltermann, A.; Schwille, P.; Eigen, M. *Proc Natl Acad Sci U S A* **1998**, *95*, 1416-20.

(16) Bacia, K.; Majoul, I. V.; Schwille, P. *Biophys. J.* **2002**, *83*, 1184-93.

(17) Bacia, K.; Kim, S. A.; Schwille, P. *Nat Methods* **2006**, *3*, 83-9.

(18) Kogure, T.; Karasawa, S.; Araki, T.; Saito, K.; Kinjo, M.; Miyawaki, A. *Nat. Biotechnol.* **2006**, *24*, 577-81.

(19) Hwang, L. C.; Wohland, T. *Chemphyschem* **2004**, *5*, 549-51.

(20) Heinze, K. G.; Koltermann, A.; Schwille, P. *Proc Natl Acad Sci U S A* **2000**, *97*, 10377-82.

(21) Burkhardt, M.; Heinze, K. G.; Schwille, P. *Opt Lett* **2005**, *30*, 2266-8.

(22) Thews, E.; Gerken, M.; Eckert, R.; Zapfel, J.; Tietz, C.; Wrachtrup, J. *Biophys. J.* **2005**, *89*, 2069-76.

(23) Anderson, J. D.; Widom, J. *J. Mol. Biol.* **2000**, *296*, 979-87.

Summary

Nucleosomes are the basic unit of DNA packaging in a eukaryotic cell. They are formed by the interaction of DNA with positively charged proteins called histones. This protein-DNA complex is a stable complex; however they are not completely static. The nucleosomal DNA unwraps from the protein core spontaneously, yet transiently before wrapping back. This transition is called site-exposure dynamics and plays an important role in gene regulation. This mechanism allows regulatory proteins to bind to their target sites which are otherwise buried in the nucleosome. The nucleosome complex also undergoes disassembly and the DNA and the proteins separate during various cellular processes. It is very important to understand the kinetics of the nucleosome dynamics and also the pathway by which the nucleosomes disassemble. This thesis aims at answering these questions.

Chapter 2 reports the study undertaken to measure the position dependent site-exposure kinetics. Using Förster resonance energy transfer (FRET) coupled with fluorescence correlation spectroscopy (FCS), we measured the site-exposure rates at various lengths of the DNA. Not all the DNA sites on a nucleosome are exposed with the same rate. Sites near the end of the nucleosomal DNA unwrap faster than the sites near the middle. The rewrapping rate also decreases along the length of the DNA but less dramatically. These results could answer cell-to-cell variation in gene expression.

Chapter 3 explores the applicability of a variation of FCS namely the Fluorescence fluctuation spectroscopy to study conformational dynamics. This method was applied to study nucleosome dynamics. Using experimental and computational validation, we proved the limitations of this method.

Chapter 4 focuses on the pathway of nucleosome disassembly induced via change in ionic strength. Nucleosome assembly/disassembly has been researched and there are questions as to what pathway is adopted by the nucleosomes. When the constituting DNA and proteins are mixed under physiological conditions, they form insoluble aggregates rather than nucleosomes. To assemble nucleosomes *in vitro*, the nucleosomes must be placed in a high ionic strength buffer (~2 M NaCl) and a step-wise dialysis must be performed to assemble the nucleosome. *In vivo* nucleosome assembly is often modeled to follow the same pathway. It is a known fact that nucleosomes disassemble upon increasing the ionic strength. However the pathway is not clearly understood. We performed dual color Fluorescence Cross-Correlation Spectroscopy (FCCS) to study the disassembly pathway.

List of Publications

1. Tims HS, **Gurunathan K**, Levitus M, Widom J “Dynamics of nucleosome invasion by DNA binding proteins” *under review*.

2. **Gurunathan K**, Levitus M (2010) "FRET Fluctuation Spectroscopy of Diffusing Biopolymers: Contributions of Conformational Dynamics and Translational Diffusion". *J. Phys. Chem. B. 114*, 980-986.

3. **Gurunathan K**, Levitus M (2009) "Single-Molecule Fluorescence Studies of Nucleosome Dynamics". *Curr. Pharm. Bio. 10*, 559-568.

4. Ranjit S, **Gurunathan K**, Levitus M (2009) "Photophysics of Backbone Fluorescent DNA Modifications: Reducing Uncertainties in FRET". *J. Phys. Chem. B . 113*, 7861-7866.

5. **Gurunathan K**, Levitus M (2008) "Applications of Fluorescence Correlation Spectroscopy to the Study of Nucleic Acid Conformational Dynamics". *Prog. Nucleic Acid Res. Mol. Biol. 82*, 33-69.

6. Sanborn ME, Connolly BK, **Gurunathan K**, Levitus M (2007) "Fluorescence Properties and Photophysics of the Sulfoindocyanine Cy3 Linked Covalently to DNA". *J. Phys. Chem. B. 111*, 1064.